Effective Models of QCD and Their Implications for Dark Matter Phenomenology

Swapnil Singh *

Posted Date: 2 December 2024

doi: 10.20944/preprints202406.1082.v2

Keywords: Effective QCD Models; Dark Matter Phenomenology; Quark-Gluon Plasma (QGP); Topological Defects and Solitons; Chiral Perturbation Theory in the Dark Sector

 doi:10.20944/preprints202406.1082.v2

Article

Effective Models of QCD and Their Implications for Dark Matter Phenomenology

Swapnil Kumar Singh

B.M.S College of Engineering, Bengaluru, Karnataka- 560019, India; swapnilsingh.ph@gmail.com

Abstract: This paper investigates the implications of effective Quantum Chromodynamics (QCD) models for dark matter phenomenology, with a particular focus on the role of QCD phase transitions, topological defects, and low-energy effective models in understanding dark matter's nature and behavior. We begin by analyzing the formation and thermodynamic properties of the quark-gluon plasma (QGP) in the early Universe, emphasizing the speed of sound c_s^2 and its effects on primordial density fluctuations, which are crucial for the formation of large-scale structures. The thermodynamic relation $c_s^2 = \frac{\partial p}{\partial \epsilon}$ is used to model the impact of these fluctuations on the evolution of the Universe. Topological structures arising from scale symmetry breaking during the rapid cooling phase of the early Universe, are explored as potential candidates for dark matter. These structures are shown to bridge the gap between QCD and cosmology, providing insights into the dark matter sector and predicting the presence of axions or other relic particles that could contribute to dark matter's observed properties. The paper also presents an in-depth study of Skyrme solitons and their potential to act as dark matter analogues. We examine the clustering dynamics of Skyrme solitons within dark matter halos, revealing a significant dependence of the soliton's energy density and stability on soliton number N and dark matter density ρ_{DM}. Numerical simulations show a strong increase in system energy as both N and ρ_{DM} are increased, highlighting the role of solitons in dark matter clustering and the formation of cosmological structures. The dynamical mass $M(T)$ of scalar fields in the presence of gravitational couplings and chemical potentials is analyzed, showing clear dependencies on the scalar field mass m_0, temperature T, and gravitational coupling G. The findings indicate that variations in the chemical potential μ lead to significant changes in mass distribution, corroborating predictions from quantum field theory (QFT) and cosmological models. Further, Chiral Perturbation Theory (ChPT) is extended to the dark sector, where SU(N) symmetries govern dark matter interactions. This extension reveals new annihilation channels for dark matter and links dark sector dynamics with cosmological observables, such as the cosmic microwave background (CMB) and dark matter relic abundance. The effect of ChPT on dark matter perturbations and large-scale structure formation is analyzed, emphasizing the role of higher-order corrections to scattering amplitudes and cross-sections in shaping the evolution of dark matter.

Keywords: effective QCD models; dark matter phenomenology; quark-gluon plasma (QGP); topological defects and solitons; chiral perturbation theory in the dark sector

1. Introduction

The search for the constituents of dark matter has spanned several decades, invoking a broad spectrum of candidates across astrophysical, cosmological, and quantum mechanical frameworks. Among the most explored candidates are Weakly Interacting Massive Particles (WIMPs), axions, sterile neutrinos, and Massive Astrophysical Compact Halo Objects (MACHOs) [1–3]. WIMPs, with predicted interactions via the weak nuclear force and masses in the range of $10\,\mathrm{GeV}/c^2 \leq m_\chi \leq 1000\,\mathrm{GeV}/c^2$, have garnered significant attention due to their compatibility with the thermal freeze-out mechanism in the early universe [1,4–6].

The evolution of the WIMP number density n_χ in the early universe is governed by the Boltzmann equation (see Figure 1):

$$\frac{dn_\chi}{dt} + 3Hn_\chi = -\langle \sigma v \rangle \left(n_\chi^2 - n_{\chi,\mathrm{eq}}^2 \right)$$

Preprints.org (www.preprints.org) | NOT PEER-REVIEWED | Posted: 2 December 2024 doi:10.20944/preprints202406.1082.v2

where $H = \frac{\dot{a}}{a}$ is the Hubble parameter, $\langle \sigma v \rangle$ represents the thermally averaged WIMP annihilation cross-section, and $n_{\chi,\text{eq}}$ is the equilibrium number density. Defining the comoving number density $Y_\chi = \frac{n_\chi}{s}$, where s is the entropy density, the equation simplifies to

$$\frac{dY_\chi}{dx} = -\frac{\langle \sigma v \rangle s}{Hx}\left(Y_\chi^2 - Y_{\chi,\text{eq}}^2\right)$$

with $x = \frac{m_\chi}{T}$, where m_χ is the mass of the WIMP and T is the temperature of the universe [7]. At high temperatures, when $x \ll 1$, the number density follows $n_\chi \sim n_{\chi,\text{eq}} \propto x^{-3/2} e^{-x}$. As the temperature drops and $x \sim 1$, annihilations cease, and n_χ freezes out at a value $Y_\chi \sim 1/x_f$, where $x_f \sim 20$ depending on $\langle \sigma v \rangle$ [5].

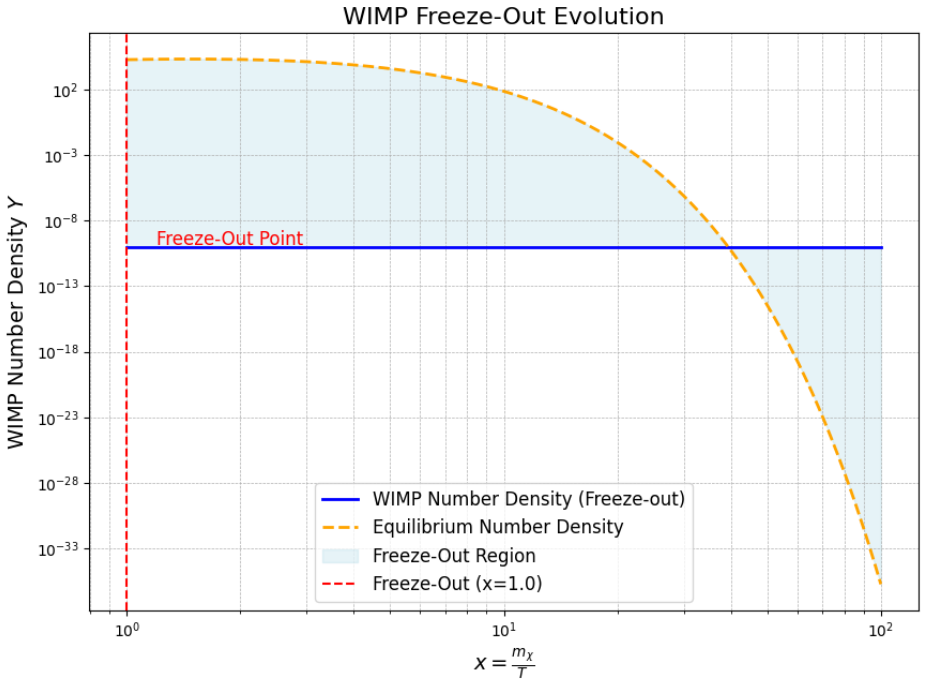

Figure 1. WIMP number density evolution during freeze-out.

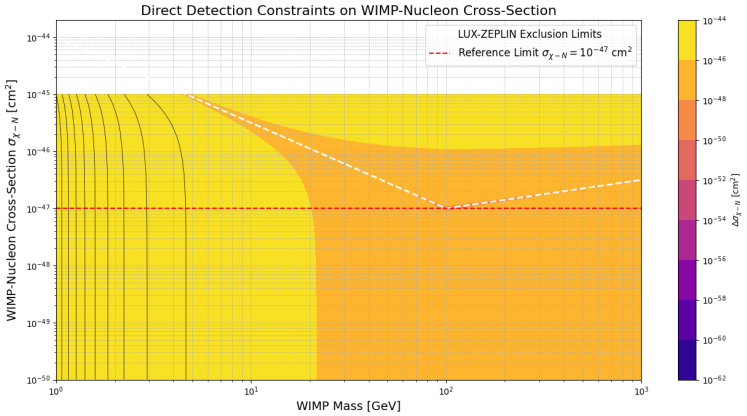

Figure 2. Direct detection constraints for WIMP-nucleon scattering cross-sections.

The relic density of WIMPs is obtained by integrating the Boltzmann equation from the freeze-out epoch to the present (see Figure 3):

 doi:10.20944/preprints202406.1082.v2

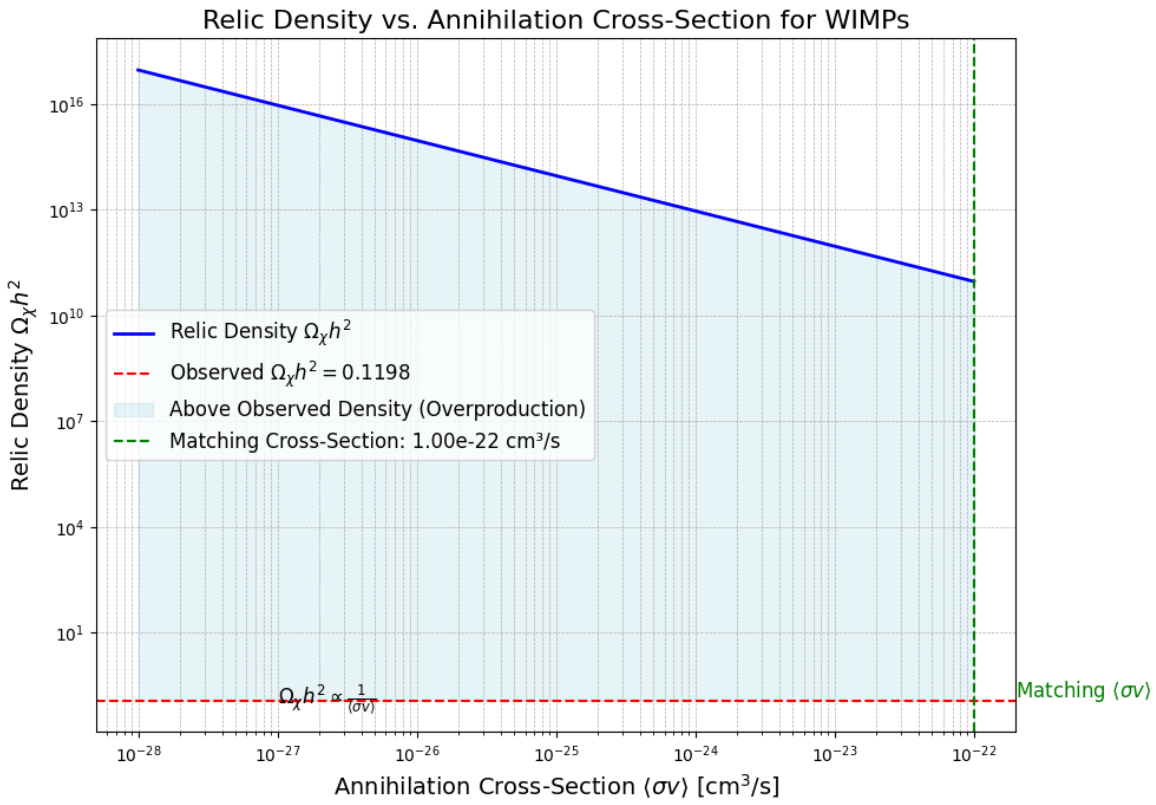

Figure 3. Relic density as a function of the annihilation cross-section.

$$\Omega_\chi h^2 = \frac{1.07 \times 10^9\,\mathrm{GeV}^{-1}}{g_*^{1/2} M_{\mathrm{Pl}}} \frac{x_f}{\langle\sigma v\rangle}$$

where g_* is the number of relativistic degrees of freedom at freeze-out, and M_{Pl} is the Planck mass. For weak-scale cross-sections $\langle\sigma v\rangle \sim 3 \times 10^{-26}\,\mathrm{cm}^3\mathrm{s}^{-1}$, this gives the observed dark matter abundance $\Omega_\chi h^2 \approx 0.12$ [8].

Despite the theoretical elegance of WIMPs, experimental searches for direct detection remain inconclusive. Direct detection experiments aim to observe nuclear recoils induced by WIMP-nucleus scattering. The differential event rate for such a process is given by

$$\frac{dR}{dE_R} = \frac{\rho_\chi}{m_\chi} \int_{v_{\min}}^{v_{\max}} d^3v\, f(v)\, v\, \frac{d\sigma}{dE_R}$$

where $\rho_\chi \approx 0.3\,\mathrm{GeV\ cm}^{-3}$ is the local dark matter density, $f(v)$ is the WIMP velocity distribution, and $\frac{d\sigma}{dE_R}$ is the differential cross-section for WIMP-nucleus scattering [9]. Stringent upper limits have been placed on the WIMP-nucleon cross-section, with LUX-ZEPLIN (LZ) setting exclusion limits down to $1.4 \times 10^{-47}\,\mathrm{cm}^2$ for a WIMP mass of $m_\chi \sim 30\,\mathrm{GeV}$ [10], while SuperCDMS explores the parameter space for lower-mass WIMPs [11].

Indirect detection strategies, such as searching for annihilation products like gamma rays or positrons, probe different regions of parameter space [12]. However, no conclusive evidence has emerged, and thus far, all WIMP search experiments have resulted in null detections, pushing the parameter space of WIMPs to increasingly constrained regimes. Additionally, anomalies such as the 130 GeV γ-ray feature in Fermi-LAT data have sparked significant debate but remain inconclusive [13].

Beyond conventional candidates, the early universe offers a fertile ground for exploring exotic configurations of dark matter. In particular, the quark-gluon plasma (QGP), formed during the quantum chromodynamics (QCD) phase transition at approximately $t \sim 10^{-5}\,\mathrm{s}$ after the Big Bang,

 doi:10.20944/preprints202406.1082.v2

provides a unique framework for generating topological defects [14,15]. These defects arise from the non-trivial vacuum structure of QCD and can exhibit stability due to topological constraints [16–21].

Topological defects are categorized by their dimensionalities:

$$\pi_n(\mathcal{M}) \neq 0 \implies \begin{cases} n = 0 & \text{(monopoles)} \\ n = 1 & \text{(strings)} \\ n = 2 & \text{(domain walls)}, \end{cases}$$

where $\pi_n(\mathcal{M})$ represents the n-th homotopy group of the vacuum manifold $\mathcal{M}$.

In the case of domain walls, their energy density per unit area σ is given by:

$$\sigma = \int_{\mathcal{M}} \left[\frac{\partial \phi}{\partial x}\right]^2 dx,$$

where $\phi(x)$ is the scalar field characterizing the defect. For flux tubes, the energy density is determined by the chromoelectric flux E_a^i:

$$\mathcal{E}_{\text{flux}} = \frac{1}{2}\int_V \left(E_a^i E_a^i\right) d^3x.$$

Additionally, quark-gluon plasma bag models predict the formation of QGP nuggets, or "quark nuggets," stabilized by surface tension and quantum pressure [22]. Quark-gluon plasma bag models predict the formation of QGP nuggets. The stability condition for the quark nuggets has been explored in various studies, indicating that stable up-down quark matter (udQM) nuggets exist under specific conditions of symmetry energy and surface tension [23–25]. Moreover, the influence of magnetic properties on the stability of these nuggets has also been considered, suggesting that ferromagnetic behavior can enhance their stability [26]. Additionally, configurational entropy has been discussed as a factor in determining the stability of compact objects, including quark nuggets [27]. The stability condition for these nuggets can be expressed as:

$$E_{\text{nugget}}(A) = a_1 A^{1/3} - a_2 A^{2/3} + a_3 A + \frac{\alpha}{A^{1/3}},$$

where A is the baryon number, and a_1, a_2, a_3, α are constants determined by the QGP properties.

Recent studies also explore the gluonic Bose-Einstein condensate (Cosmic Gluonic Background, CGB) as a dark matter candidate, formed due to the QCD trace anomaly [28–32]. The energy density of the CGB, ρ_{CGB}, is governed by the QCD vacuum expectation value:

$$\rho_{\text{CGB}} = \langle T_\mu^\mu \rangle_{\text{QCD}},$$

where T_μ^μ is the trace of the QCD energy-momentum tensor.

This paper examines the hypothesis that topological defects formed during the QCD phase transition could constitute dark matter, with a focus on their dynamical stability, interactions with baryonic matter, and cosmological implications.

In particular, we examine the Skyrme model, a classical effective field theory that predicts topologically stable solitons, and explore their cosmological implications as analogs for dark matter. We extend this discussion to the Nambu-Jona-Lasinio model, focusing on the formation and dynamics of domain walls as potential dark matter candidates.

The effects of these defects on heavy quarkonium dissociation in an anisotropic QGP have been investigated, revealing significant shifts in dissociation energies [16–21,33]:

$$\Delta E_{\text{diss}} = \frac{\alpha_s}{r} - \frac{\sigma r}{2},$$

 doi:10.20944/preprints202406.1082.v2

where α_s is the strong coupling constant, r is the quarkonium radius, and σ is the string tension. These results suggest profound implications for the evolution of the early universe and the nature of dark matter.

2. Quark-Gluon Plasma in the Early Universe

Quark-gluon plasma (QGP) is a deconfined phase of quantum chromodynamics (QCD) matter, characterized by the liberation of quarks and gluons from their hadronic confines [14]. This state is hypothesized to have existed during the initial microseconds following the Big Bang, when the Universe's temperature exceeded the QCD deconfinement scale, $T_c \sim 150$–200 MeV [34,35]. The study of QGP not only deepens our understanding of the strong interaction but also serves as a window into the conditions of the early Universe [35–39].

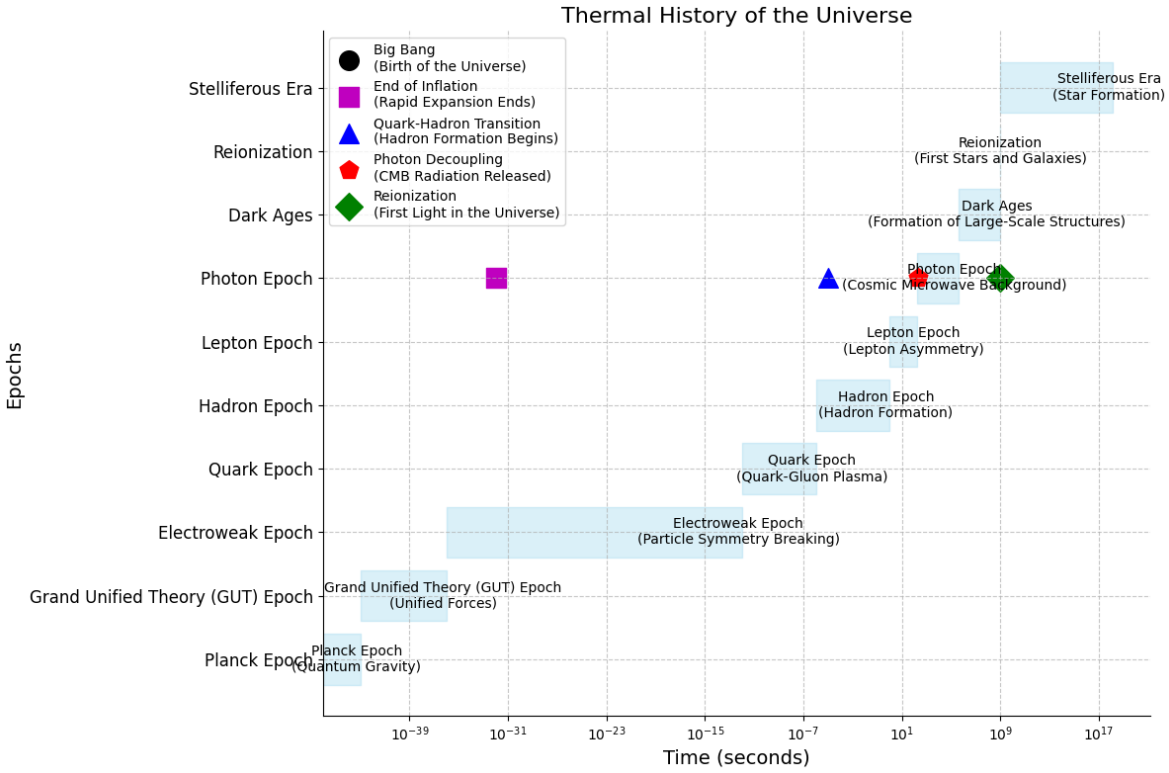

Figure 4. Thermal History of the Universe. The figure depicts the transition epochs, including the QCD phase transition where quarks and gluons were deconfined in the early Universe.

2.1. QCD Thermodynamics and QGP Formation

In QCD, the thermodynamic behavior of strongly interacting matter is encapsulated in the partition function:

$$\mathcal{Z} = \int \mathcal{D}A\mathcal{D}\bar{\psi}\mathcal{D}\psi\, e^{-S_{\text{QCD}}[A,\bar{\psi},\psi]}, \tag{1}$$

where S_{QCD} is the Euclidean QCD action given by:

$$S_{\text{QCD}} = \int d^4x \left[\frac{1}{4}F^a_{\mu\nu}F^{\mu\nu}_a + \bar{\psi}(i\gamma^\mu D_\mu - m)\psi\right]. \tag{2}$$

Here, $F^a_{\mu\nu}$ is the gluon field tensor, ψ represents the quark fields, and D_μ is the covariant derivative [34,40]. At temperatures $T \gg T_c$, the expectation value of the Polyakov loop $\langle L(\vec{x})\rangle$ transitions from $\langle L\rangle = 0$ (confined phase) to $\langle L\rangle \neq 0$ (deconfined phase), signaling QGP formation [41,42]. Modern studies using lattice QCD simulations provide precise insights into the equation of state and the nature of the phase transition [39,43–46].

 doi:10.20944/preprints202406.1082.v2

2.2. Transport Properties of QGP

The QGP exhibits unique transport properties, characterized by a near-minimal shear viscosity to entropy density ratio:

$$\frac{\eta}{s} \gtrsim \frac{1}{4\pi}, \tag{3}$$

where $1/4\pi$ is the conjectured lower bound derived from the AdS/CFT correspondence [43–48]. The small value of η/s implies a nearly perfect fluidity, which manifests in collective flow phenomena such as elliptic flow.

The energy density $\epsilon(T)$ and pressure $p(T)$ of QGP are governed by the equation of state derived from lattice QCD:

$$\frac{\epsilon - 3p}{T^4} = \frac{1}{T^4}\left(T\frac{\partial p}{\partial T} - 4p\right). \tag{4}$$

The rapid rise in $\epsilon(T)$ near T_c reflects the deconfinement transition and the liberation of partonic degrees of freedom [43–46,48,49].

2.3. Experimental Observables and Theoretical Models

Heavy-ion collision experiments probe the quark-gluon plasma (QGP) by creating a fireball of high-energy density. The space-time evolution of this fireball is modeled by relativistic hydrodynamics [50,51], governed by the equation:

$$\partial_\mu T^{\mu\nu} = 0, \tag{5}$$

where $T^{\mu\nu}$ is the energy-momentum tensor, expressed as:

$$T^{\mu\nu} = (\epsilon + p)u^\mu u^\nu - pg^{\mu\nu} + \pi^{\mu\nu}, \tag{6}$$

with u^μ as the fluid velocity and $\pi^{\mu\nu}$ representing the viscous stress tensor [52,53]. Elliptic flow, quantified by the Fourier coefficient v_2, serves as a key observable for the QGP [54,55]:

$$v_2 = \frac{\int d\phi \cos(2\phi)\frac{dN}{d\phi}}{\int d\phi \frac{dN}{d\phi}}, \tag{7}$$

where ϕ is the azimuthal angle of emitted particles.

2.4. Jet Quenching and Energy Loss Mechanisms

Jet quenching provides direct evidence for the dense medium created in heavy-ion collisions. The energy loss of a high-energy parton traversing the QGP is described by the Baier-Dokshitzer-Mueller-Peigné-Schiff (BDMPS) framework [56], which predicts that:

$$\Delta E \propto \hat{q}L^2, \tag{8}$$

where $\hat{q}$ is the jet transport coefficient, and L is the path length through the medium [57]. Suppression of high-transverse-momentum particles, quantified by the nuclear modification factor R_{AA}, serves as a hallmark of QGP [48]:

$$R_{AA} = \frac{d^2N^{\mathrm{AA}}/dp_T d\eta}{\langle N_{\mathrm{coll}}\rangle d^2N^{\mathrm{pp}}/dp_T d\eta}. \tag{9}$$

Additionally, azimuthal anisotropy in particle emission, often quantified using the elliptic flow coefficient v_2, provides further insights into the properties of the QGP [54].

 doi:10.20944/preprints202406.1082.v2

2.5. Cosmological Implications

The study of the quark-gluon plasma (QGP) offers profound insights into the thermodynamic evolution of the early Universe, particularly during the quantum chromodynamics (QCD) phase transition [58,59]. During this epoch, the speed of sound, c_s, in the primordial plasma is given by

$$c_s^2 = \frac{\partial p}{\partial \epsilon}, \tag{10}$$

where p is the pressure and ϵ is the energy density of the plasma [60,61]. Significant changes in c_s during the QCD phase transition affected the evolution of primordial density fluctuations, playing a crucial role in the formation of large-scale structures [61].

Moreover, the rapid cooling of the Universe could have resulted in the formation of topological defects, such as domain walls or cosmic strings, arising from symmetry-breaking processes [62,63]. These defects are hypothesized to contribute to dark matter candidates, such as axions or other relic particles, depending on the nature of the QCD phase transition [22,64].

The QGP also serves as a probe for extreme conditions of quantum chromodynamics, offering unique opportunities to connect the microphysics of heavy-ion collisions to macroscopic cosmological phenomena. Its study continues to challenge our understanding of fundamental physics and the interplay between particle physics and cosmology [37,65].

3. Topological Structures in QCD and Their Role in Dark Matter Physics

The hypothesis that Quantum Chromodynamics (QCD) may harbor topological structures, such as flux tubes, domain walls, or monopoles, presents an intriguing avenue for understanding the non-perturbative dynamics of the strong interaction. Furthermore, the potential connection between these structures and dark matter warrants a detailed exploration, provided the assertions are grounded in robust theoretical and mathematical frameworks. Here, we critically examine this hypothesis through the lens of gauge theory, lattice QCD, and effective field theory while addressing the fundamental issues raised in the literature [22,35,62,63,66–77].

3.1. Theoretical Foundations and Scale Symmetry Breaking

QCD, as a non-Abelian gauge theory described by the Lagrangian

$$\mathcal{L}_{\text{QCD}} = -\frac{1}{4} F^a_{\mu\nu} F_a^{\mu\nu} + \bar{\psi}_f \left(i\gamma^\mu D_\mu - m_f \right) \psi_f, \tag{11}$$

is classically scale-invariant, where $F^a_{\mu\nu} = \partial_\mu A^a_\nu - \partial_\nu A^a_\mu + g f^{abc} A^b_\mu A^c_\nu$ is the gluon field strength tensor, A^a_μ represents the gauge fields, and ψ_f denotes the quark fields of flavor f. Quantum corrections, however, introduce a scale through the renormalization group equation:

$$\mu \frac{\mathrm{d}g}{\mathrm{d}\mu} = \beta(g) = -\beta_0 g^3 - \beta_1 g^5 + \mathcal{O}(g^7), \tag{12}$$

where $\beta_0 = \frac{11N_c - 2N_f}{48\pi^2}$ reflects the asymptotic freedom of QCD [66]. This scale-breaking effect, encapsulated in the QCD scale Λ_{QCD}, raises the possibility of non-trivial vacuum structures, such as a quark-gluon condensate:

$$\langle 0 | \bar{\psi} \psi | 0 \rangle \neq 0. \tag{13}$$

While these features suggest rich vacuum dynamics, the emergence of extended topological defects remains highly speculative [76].

 doi:10.20944/preprints202406.1082.v2

3.2. Gauge-Invariant Formulation of Confinement and Flux Tubes

The confinement phenomenon in QCD, characterized by the linear growth of the potential between quarks,

$$V(r) = \sigma r + \mathcal{O}(1/r), \tag{14}$$

where σ is the string tension, is often interpreted in terms of gluon flux tubes [69]. These flux tubes correspond to solutions of the Wilson loop operator:

$$W(C) = \left\langle \mathrm{Tr}\, \mathcal{P} \exp\left(ig \oint_C A_\mu^a T^a \, \mathrm{d}x^\mu \right) \right\rangle \propto e^{-\sigma A(C)}, \tag{15}$$

where C is a closed loop, $\mathcal{P}$ denotes path ordering, and $A(C)$ is the minimal area spanned by C. However, these flux tubes are not independent topological objects; they exist solely as part of the quark confinement mechanism. The absence of gauge-invariant classical solutions for free-standing flux tubes challenges their identification as topological defects [68].

3.3. Low-Energy Effective Models and Solitonic Solutions

In contrast to QCD itself, several low-energy effective models, such as the Skyrme model [70], offer solitonic solutions with potential implications for dark matter. The Skyrme Lagrangian,

$$\mathcal{L}_{\text{Skyrme}} = \frac{f_\pi^2}{4} \mathrm{Tr}\left(\partial_\mu U \partial^\mu U^\dagger \right) + \frac{1}{32e^2} \mathrm{Tr}\left(\left[U^\dagger \partial_\mu U, U^\dagger \partial_\nu U \right]^2 \right), \tag{16}$$

admits soliton solutions, or Skyrmions, which carry topological charge:

$$Q = \frac{1}{24\pi^2} \int \epsilon^{ijk} \mathrm{Tr}\left(U^\dagger \partial_i U U^\dagger \partial_j U U^\dagger \partial_k U \right) \mathrm{d}^3 x. \tag{17}$$

These structures, while mathematically well-defined, are derived from an effective theory and do not necessarily imply analogous structures in QCD itself [71].

3.4. Nambu–Jona-Lasinio Model and Dark Matter

The NJL model, developed to describe spontaneous chiral symmetry breaking in QCD [78,79], provides another framework for exploring dark matter candidates. The model is characterized by a four-fermion interaction:

$$\mathcal{L}_{\text{NJL}} = \bar{\psi}(i\gamma^\mu \partial_\mu - m)\psi + g\left((\bar{\psi}\psi)^2 + (\bar{\psi} i\gamma_5 \tau \psi)^2 \right), \tag{18}$$

where ψ is the quark field and g is a coupling constant. The spontaneous symmetry breaking in the NJL model gives rise to fermionic condensates, which could contribute to the formation of dark matter-like states, such as dark mesons or light baryons [77,80].

3.5. Chiral Perturbation Theory and Dark Matter Models

Chiral perturbation theory (ChPT) is the effective field theory of QCD that describes the dynamics of pions and other pseudo-Goldstone bosons. The Lagrangian of ChPT, at lowest order, is given by:

$$\mathcal{L}_{\text{ChPT}} = \frac{f_\pi^2}{4} \mathrm{Tr}\left(\partial_\mu U \partial^\mu U^\dagger \right) + \cdots, \tag{19}$$

where $U(x)$ is the pion field and f_π is the pion decay constant. ChPT provides a useful framework for describing low-energy QCD interactions, which are important for constructing models of dark matter that may interact via pseudo-scalar mediators [81,82].

The effective models of QCD, such as the Skyrme model, NJL model, and ChPT, provide a rich landscape for exploring the nature of dark matter. Their solitonic solutions, clustering behaviors, and

 doi:10.20944/preprints202406.1082.v2

potential gravitational signatures offer intriguing possibilities for dark matter analogs. Continued advancements in numerical simulations, coupled with observational probes like gravitational waves, will be key to verifying these models as viable candidates for dark matter.

3.6. Dark Matter Implications and Future Work

The role of topological structures in dark matter physics requires cautious interpretation. To draw meaningful connections, one must first identify physically realizable solutions within QCD or its extensions. Promising avenues include holographic QCD, where flux tubes emerge as string-like configurations in higher-dimensional spacetimes [72], and lattice studies of gluonic configurations under extreme conditions [73]. Ultimately, progress in this domain hinges on combining rigorous mathematical frameworks with state-of-the-art computational techniques [62,74,75].

Although the existence of topological defects in QCD remains unproven, the exploration of analogous structures in effective field theories and specialized contexts offers valuable insights. Future research must rigorously delineate between speculative analogies and physical phenomena, fostering a more robust understanding of the interplay between QCD, confinement, and dark matter.

4. Classical Solutions in Effective Models of QCD and Their Relevance to Dark Matter

Low-energy effective models of quantum chromodynamics (QCD), such as the Skyrme model [83], the Nambu–Jona-Lasinio (NJL) model [78,79], and chiral perturbation theory (ChPT) [81], offer valuable insights into non-perturbative phenomena. These models capture exotic dynamics like solitons, domain walls, and flux tubes, characterized by localized energy densities and remarkable stability properties. While initially developed to elucidate hadronic physics, their stability and interactions within the Standard Model (SM) provide intriguing parallels to dark matter (DM) candidates. Here, we explore the theoretical, computational, and astrophysical implications of these effective QCD models, focusing on their relevance for dark matter analogs.

4.1. Skyrme Model: Topological Solitons as Analogues of Dark Matter

The Skyrme model [83] represents one of the most studied field-theoretic frameworks for baryons, supporting topologically stable solitons termed Skyrmions. These solitons are characterized by a nontrivial topological charge, which stabilizes their structure and renders them analogous to dark matter: non-luminous, robust, and capable of clustering [84,85]. The model's Lagrangian density is given by:

$$\mathcal{L}_{\text{Skyrme}} = \frac{f_\pi^2}{4}\text{Tr}(\partial_\mu U \partial^\mu U^\dagger) + \frac{1}{32e^2}\text{Tr}\Big([U^\dagger \partial_\mu U, U^\dagger \partial_\nu U]^2\Big), \tag{20}$$

where $U(x) \in \text{SU}(2)$ is the pion field, f_π is the pion decay constant, and e is a dimensionless coupling constant. The non-linear Euler-Lagrange equations derived from this Lagrangian yield stable field configurations corresponding to the Skyrmions. The Skyrme model's potential to describe baryons as solitons was initially explored by Adkins, Nappi, and Witten [86], and it has since been expanded to include interactions with vector mesons [87].

4.1.1. Topological Charge and Stability

Skyrmions are stabilized by a topological charge B, which is typically identified with the baryon number. This topological charge is quantized, ensuring solitonic stability and an analogy with the long-lived nature of dark matter halos in astrophysics [85,88]. The topological charge is given by:

$$B = \frac{1}{24\pi^2}\int_{\mathbb{R}^3} \epsilon^{ijk}\text{Tr}\Big((U^\dagger \partial_i U)(U^\dagger \partial_j U)(U^\dagger \partial_k U)\Big) d^3x, \tag{21}$$

which can be interpreted as a conserved quantity under suitable boundary conditions. The quantization of B leads to stable solitonic solutions, analogous to the stability of dark matter structures in the universe.

 doi:10.20944/preprints202406.1082.v2

4.1.2. Energy Density and Compactness

Numerical simulations of the Skyrme model reveal that Skyrmions possess compact, localized energy configurations with a characteristic size given by:

$$R \sim \frac{1}{f_\pi e}. \tag{22}$$

These configurations exhibit the dense, non-luminous properties characteristic of dark matter [89,90]. The energy density is typically concentrated in a small region, reflecting the behavior of dark matter halos, which are observed to be diffuse yet dense at their cores.

4.1.3. Skyrmion Clustering and Cosmological Implications

Skyrmions interact via a potential V_{int} that facilitates clustering, similar to the formation of dark matter halos. The interaction potential between two Skyrmions is modeled as:

$$V_{\text{int}}(r) \sim -\frac{c_1}{r^2} + \frac{c_2}{r^6}, \quad r \gg R, \tag{23}$$

where the first term represents the attractive interaction at short distances, and the second term captures the repulsive behavior at large distances. These interactions lead to bound-state configurations, similar to the clustering of dark matter in cosmological simulations [88,91]. Multi-Skyrmion configurations can form lattice structures, mimicking the self-gravitating dynamics observed in dark matter simulations [85,91].

4.1.4. Extensions and Future Directions

The Skyrme model can be extended by introducing higher-order terms or coupling to vector mesons, enhancing its applicability to astrophysical scenarios [85,87]. Furthermore, embedding the Skyrme model in the AdS/CFT framework offers a promising route to understanding its behavior in the strong-coupling regime, potentially shedding light on the behavior of dark matter at higher energies [92]. Future research should focus on:

- The production mechanisms of Skyrmions in the early universe [77].
- Gravitational wave signatures from Skyrmion clusters, which could provide a new observational probe for dark matter [93].
- The reconciliation of Skyrmion masses with current dark matter constraints, as Skyrmion mass distributions are typically non-thermal [77].

Simulations incorporating Skyrmion dynamics with general relativity will play a critical role in addressing these questions, providing key insights into the potential role of Skyrmions as dark matter candidates [94].

4.1.5. Simulating Skyrme Solitons and Dark Matter Halo Interactions

This section details the numerical simulation of Skyrme solitons interacting with a dark matter halo described by an NFW (Navarro-Frenk-White) profile [95]. The dynamics of the soliton field are computed by solving the coupled Skyrme and gravitational potential equations, employing a Runge-Kutta numerical integrator for time evolution.

The Skyrme field $U(x)$ is modeled using the hedgehog ansatz for the $SU(2)$ field, with energy density given by [96]:

$$\mathcal{E} = \frac{f_\pi^2}{4}\left(|\nabla U|^2\right) + \frac{1}{32e^2}|[U, \nabla U]|^2,$$

where f_π and e are Skyrme parameters [83,96]. The gravitational potential from the NFW dark matter profile is:

$$\Phi(r) = -\frac{G\rho_0}{r}\ln\left(1 + \frac{r}{r_s}\right),$$

 doi:10.20944/preprints202406.1082.v2

where ρ_0 and r_s characterize the halo's density profile [95]. The equations of motion for U are solved in polar coordinates on a spatial grid with periodic boundary conditions.

The system is initialized with N Skyrme solitons distributed randomly in a 10 fm $\times$ 10 fm box. Parameters include $f_\pi = 93.0\,\text{MeV}, e = 4.0, \rho_0 = 1.0\,\text{MeV/fm}^3$, and $r_s = 2.0\,\text{fm}$. A timestep of $\Delta t = 0.01\,\text{fm}/c$ is used to evolve the field for $t_{\max} = 5.0\,\text{fm}/c$.

Simulations with $N = 15$ and $N = 30$ solitons reveal clustering driven by the dark matter halo. The energy density distribution at $t = t_{\max}$ shows tighter soliton configurations as N increases, with total energy scaling approximately as $E \propto N^2$, the soliton core properties depend critically on both the self-gravity of the soliton and the external potential of the host halo[97]. For $N = 15$, the central energy density peaks at $1.2 \times 10^7\,\text{MeV}^4$, while for $N = 30$, it reaches $6.2 \times 10^7\,\text{MeV}^4$. These results suggest enhanced gravitational binding of solitons due to the increased halo density.

Energy profiles along x- and y-axes confirm that soliton interactions with the dark matter potential induce anisotropies, with maximum energy values occurring near the soliton cores. The higher ρ_0 configurations lead to pronounced clustering, consistent with theoretical predictions of soliton self-interaction in external potentials, steady interaction occurs when the crest of the soliton and the crest of the external force are in phase [98].

Figures 5 and 6 illustrate the energy density for $N = 15$ and $N = 30$, respectively, highlighting the effect of soliton number on system stability.

Additionally, we compare the energy profiles along the x-axis and y-axis for the two sets of simulations. These comparisons, shown in Figures 7 and 8, provide insight into how the soliton configurations influence the overall energy distribution.

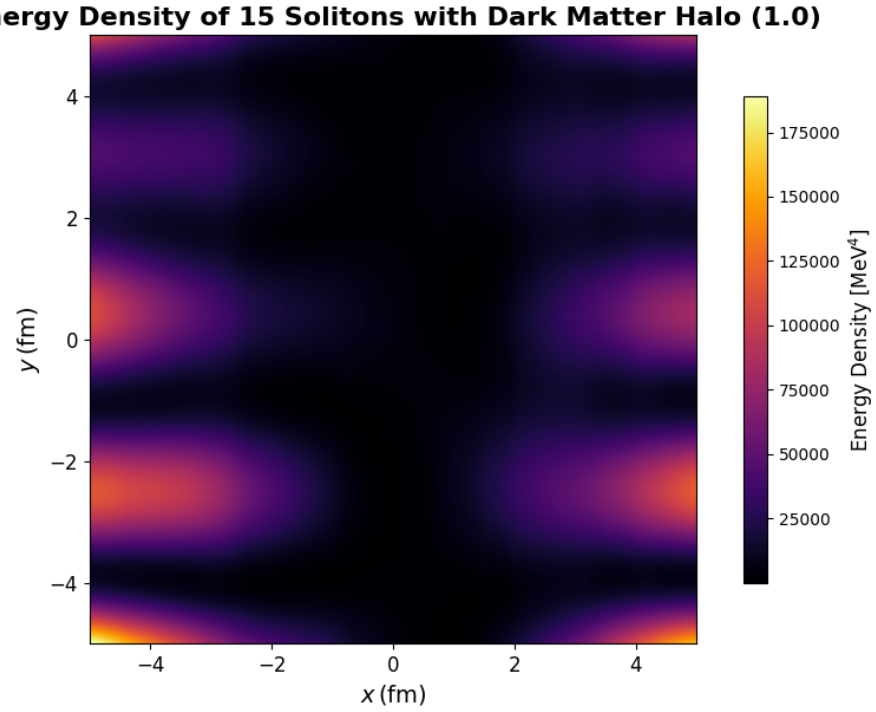

Figure 5. Energy density of 15 Skyrme solitons interacting with a dark matter halo.

 doi:10.20944/preprints202406.1082.v2

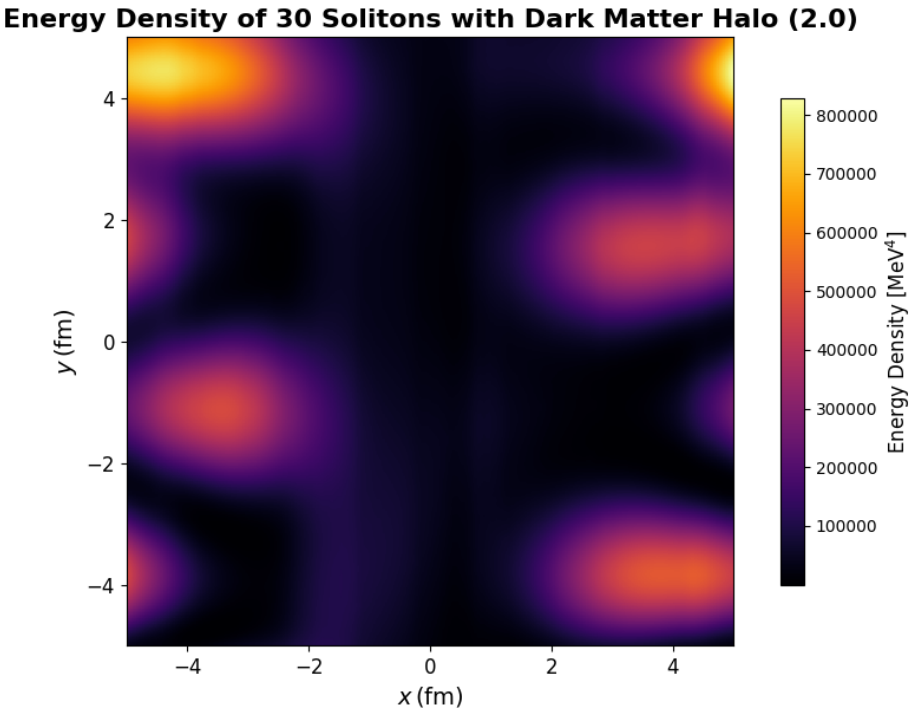

Figure 6. Energy density of 30 Skyrme solitons interacting with a dark matter halo.

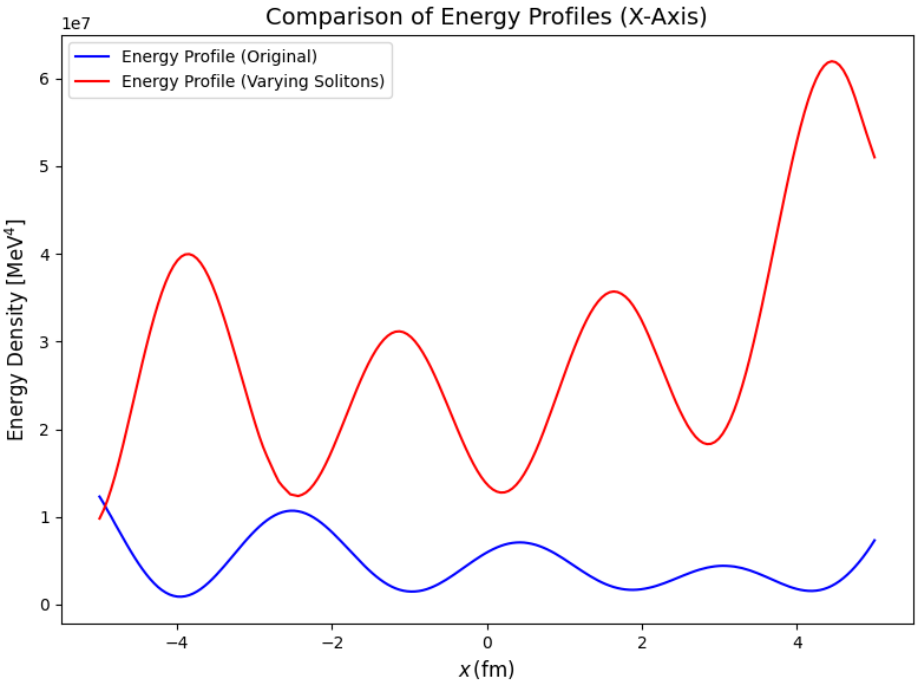

Figure 7. Energy profile along the x-axis for 15 solitons (blue) and 30 solitons (red).

Preprints.org (www.preprints.org) | NOT PEER-REVIEWED | Posted: 2 December 2024 doi:10.20944/preprints202406.1082.v2

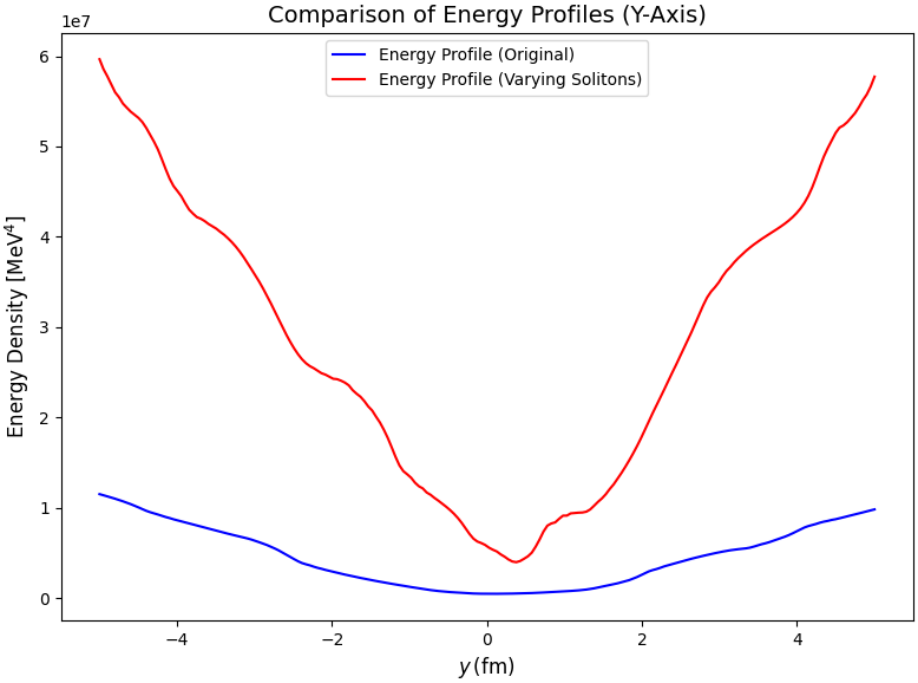

Figure 8. Energy profile along the y-axis for 15 solitons (blue) and 30 solitons (red).

At the final time step, the total energy for the configuration with 15 solitons and dark matter density $\rho_{\mathrm{DM}} = 1.0\,\mathrm{MeV/fm^3}$ was $9.1378 \times 10^8\,\mathrm{MeV^4}$, while for 30 solitons and $\rho_{\mathrm{DM}} = 2.0\,\mathrm{MeV/fm^3}$, it was $5.7541 \times 10^9\,\mathrm{MeV^4}$, showing an almost 10-fold increase with denser dark matter and more solitons. This suggests that both increased soliton number and dark matter density strengthen interactions within the system.

Energy profiles along the x- and y-axes reveal the spatial energy distribution. For the 15 soliton case, the x-axis profile showed a peak of $1.2315 \times 10^7\,\mathrm{MeV^4}$ and a minimum of $9.0061 \times 10^5\,\mathrm{MeV^4}$, with similar trends along the y-axis. In the 30 soliton configuration, the maximum energy along the x-axis increased to $6.1964 \times 10^7\,\mathrm{MeV^4}$, with a corresponding rise in the minimum energy, reflecting stronger energy clustering due to the denser dark matter halo.

Energy values at the grid center were also higher for the 30 soliton case. For 15 solitons, the central energy was $6.0778 \times 10^6\,\mathrm{MeV^4}$ along the x-axis and $4.6506 \times 10^5\,\mathrm{MeV^4}$ along the y-axis. In contrast, for 30 solitons, the central energy increased to $1.3490 \times 10^7\,\mathrm{MeV^4}$ along the x-axis and $5.5722 \times 10^6\,\mathrm{MeV^4}$ along the y-axis, indicating stronger soliton clustering and more pronounced dark matter effects.

Table 1. Total Energy Comparison.

Configuration	**Total Energy** ($\mathrm{MeV^4}$)
15 solitons, $\rho_{\mathrm{DM}} = 1.0\,\mathrm{MeV/fm^3}$	9.1378×10^8
30 solitons, $\rho_{\mathrm{DM}} = 2.0\,\mathrm{MeV/fm^3}$	5.7541×10^9

Energy density plots for the 15 soliton configuration show more diffuse energy distribution with localized peaks, while the 30 soliton configuration exhibits a denser, more tightly bound energy distribution. The sharper, higher peaks in the 30 soliton case highlight the stronger soliton-dark matter interactions and suggest a more stable, clustered system.

This demonstrates a stronger clustering of solitons in the denser dark matter configuration, with a much higher central energy concentration. The sharper peaks in the energy profiles for the 30 soliton configuration further confirm the enhanced soliton interactions and the more energetically dense system.

 doi:10.20944/preprints202406.1082.v2

These results highlight the gravitational coupling between Skyrme solitons and dark matter halos, showcasing the clustering and energy density amplification effects under varying soliton numbers and halo densities.

4.2. The Nambu-Jona-Lasinio Model: A Dynamical Framework for Chiral Symmetry Breaking

The Nambu-Jona-Lasinio (NJL) model is a relativistic quantum field theory framework that encapsulates the dynamics of fermionic fields interacting through four-fermion interactions, providing a phenomenological description of dynamical mass generation and spontaneous chiral symmetry breaking. Originally proposed by Nambu and Jona-Lasinio in 1961 [78,79], this model has played a central role in the development of effective field theories in the low-energy limit of quantum chromodynamics (QCD), where quark-gluon dynamics becomes non-perturbative.

The NJL model is governed by the following effective Lagrangian density [99]:

$$\mathcal{L} = \bar{\psi}(i\partial\!\!\!/ - m_0)\psi + G\Big[(\bar{\psi}\psi)^2 + (\bar{\psi}i\gamma_5\psi)^2\Big], \tag{24}$$

where ψ is a Dirac spinor field representing the fermions, m_0 is the bare fermion mass, and G is the coupling constant. The second term describes the interaction between fermions and their chiral partners, which is responsible for the spontaneous breaking of chiral symmetry in the vacuum. The parameter G governs the strength of this interaction and is usually considered to be a running coupling constant.

Within the mean-field approximation, the fermion condensate $\langle\bar{\psi}\psi\rangle$ induces a dynamical mass for the fermion field, which can be determined by solving the gap equation:

$$M = m_0 + G\langle\bar{\psi}\psi\rangle. \tag{25}$$

The condensate $\langle\bar{\psi}\psi\rangle$ is a non-perturbative order parameter that signifies the spontaneous breaking of chiral symmetry. The presence of such a condensate leads to the generation of a fermionic mass M and provides a theoretical basis for the low-energy dynamics of strongly interacting fermions, such as the quarks in QCD [99–101].

The solution to the gap equation at finite temperature and density involves the computation of the fermionic determinant, typically requiring the use of numerical techniques or an expansion in the strong-coupling limit. In the limit of large N_c (the number of colors), the NJL model can be solved analytically, but for finite N_c, numerical methods are often employed.

4.2.1. Domain Walls in the Nambu-Jona-Lasinio Model

The NJL model, under certain conditions, admits non-trivial classical solutions such as domain walls [102]. Domain walls are topological defects that arise during spontaneous symmetry breaking when distinct vacuum states separated by finite energy barriers coexist [62,63].

A domain wall is a one-dimensional defect in a two-dimensional field space, characterized by a non-trivial configuration of the scalar field, such that the field interpolates between two distinct vacuum states. In the context of the NJL model, domain walls can be associated with the spatially dependent chiral condensate. The presence of a non-trivial field profile within the wall structure indicates a region where the vacuum structure changes in space.

To explore the structure of domain walls in the NJL model, we consider the scalar field theory with the potential

$$V(\phi) = \lambda(\phi^2 - v^2)^2, \tag{26}$$

Preprints.org (www.preprints.org) | NOT PEER-REVIEWED | Posted: 2 December 2024 doi:10.20944/preprints202406.1082.v2

where ϕ represents the scalar field and v is the vacuum expectation value (VEV) (see Figure 9). The configuration of the domain wall solutions for the scalar field $\phi(x)$ is then governed by the equation of motion derived from the Euler-Lagrange equation for the field:

$$\frac{d^2\phi}{dx^2} = \frac{dV(\phi)}{d\phi} = 4\lambda(\phi^2 - v^2)\phi. \tag{27}$$

The solution to this equation, subject to boundary conditions $\phi(x \to \infty) = v$ and $\phi(x \to -\infty) = -v$, is given by the well-known kink solution [103]:

$$\phi(x) = v \tanh\left(\frac{x}{\delta}\right), \tag{28}$$

where $\delta = 1/(\sqrt{\lambda}v)$ represents the characteristic thickness of the domain wall. This solution describes a topologically stable configuration that interpolates between two distinct vacua [102]. The domain wall energy density is concentrated within the width δ and is associated with the tension σ, which is proportional to the integral of the potential:

$$\sigma \sim \int dx \left[\frac{1}{2}\left(\frac{d\phi}{dx}\right)^2 + V(\phi)\right]. \tag{29}$$

This energy density scales with the coupling constant λ and the vacuum expectation value v, and represents the energy required to create the domain wall in the theory.

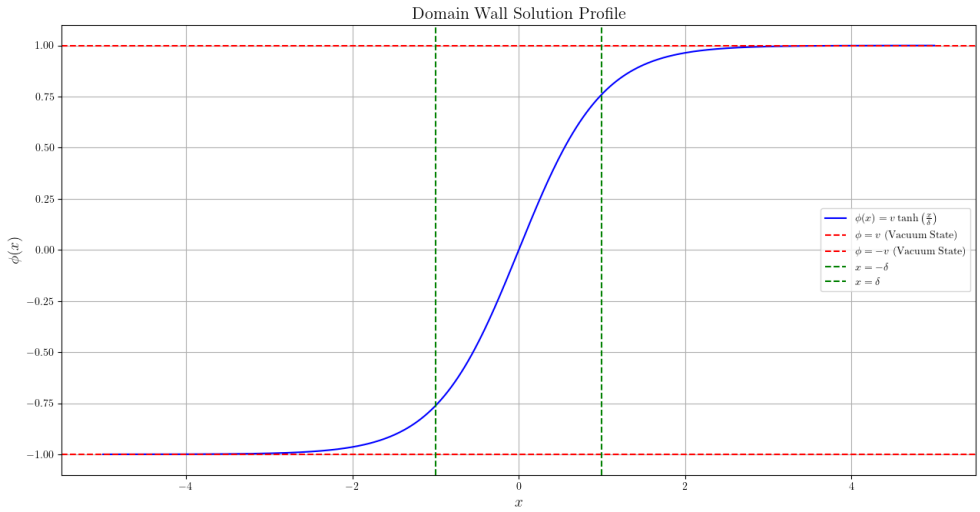

Figure 9. Domain Wall Solution Profile.

4.2.2. Domain Wall Dynamics in the Nambu-Jona-Lasinio Model

To study the behavior of domain walls in the Nambu-Jona-Lasinio (NJL) model, we performed a numerical simulation of the domain wall dynamics under the influence of the scalar field potential. The evolution of the scalar field $\phi(x,t)$ was tracked over time to examine the amplitude, energy, and spatial structure of the domain walls.

The scalar field evolves according to the equation:

$$\frac{\partial^2\phi}{\partial t^2} = \frac{\partial^2\phi}{\partial x^2} - \frac{dV(\phi)}{d\phi}, \tag{30}$$

 doi:10.20944/preprints202406.1082.v2

where the potential $V(\phi) = \lambda(\phi^2 - v^2)^2$ governs the dynamics. The equation was solved numerically using finite-difference methods on a spatial grid, with boundary conditions $\phi(x \to \infty) = v$ and $\phi(x \to -\infty) = -v$.

The simulation results show that the maximum amplitude of the scalar field is 2.4282, and the time-averaged energy of the system is 6.2595×10^3. The damping factor, which describes the ratio of the final to the initial amplitude, is 0.8672, indicating a decrease in amplitude over time. At $t = 5.00\,\text{s}$, the domain wall is located at $x = 8.9780\,\text{m}$, with a domain wall thickness of 10.0000 m.

Figures 10 and 11 show the results. Figure 10 illustrates the scalar field profile, showing the transition between the two vacuum states as the domain wall evolves. The kink solution, representing the domain wall, is visible in the figure. Figure 11 shows the energy density distribution of the domain wall at $t = 5.00\,\text{s}$.

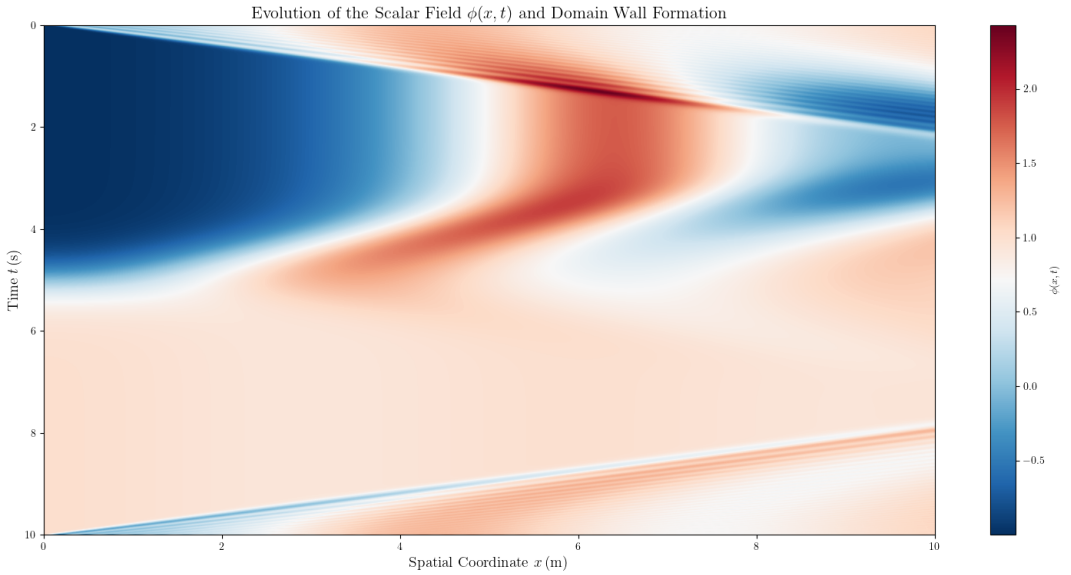

Figure 10. Time evolution of the domain wall position and scalar field profile.

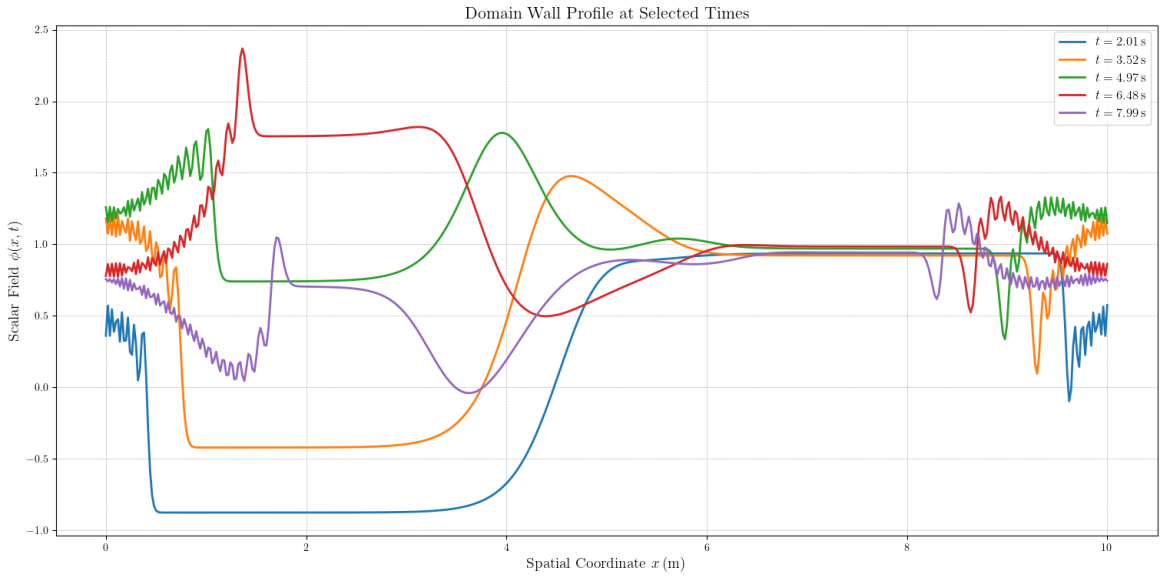

Figure 11. Energy density distribution of the domain wall at $t = 5.00\,\text{s}$.

Preprints.org (www.preprints.org) | NOT PEER-REVIEWED | Posted: 2 December 2024 doi:10.20944/preprints202406.1082.v2

The domain wall stabilizes into a defined structure, with its position and thickness remaining stable after an initial period of evolution. The damping factor reflects the typical relaxation behavior, where the field eventually settles into a minimal energy configuration.

These results are relevant for understanding domain walls as topological defects in the NJL model. Given their stability, domain walls could be important candidates for dark matter, as they may persist over cosmological timescales and interact weakly with standard model particles.

While this simulation provides crucial insights into the behavior of domain walls in the NJL model, further investigations are required to fully understand their cosmological implications. Detailed numerical simulations that incorporate the interactions of domain walls with other matter fields and their contributions to large-scale structure formation are essential.

4.2.3. Domain Walls as Dark Matter Candidates

The potential of domain walls as candidates for dark matter arises from their unique topological properties and their ability to remain stable over cosmological time scales. Domain walls can be produced during symmetry-breaking phase transitions in the early universe, and their topological stability means that they are not easily annihilated by standard model particles, unlike other forms of matter [104,105].

For domain walls to be viable dark matter candidates, their energy density must be consistent with the observed value of dark matter in the universe. The energy density of a domain wall network evolves as (see Figure 12):

$$\rho_{\mathrm{DW}}(t) \propto \frac{\sigma}{t}, \tag{31}$$

where t is the cosmic time, and σ is the domain wall tension. This evolution suggests that domain walls can be a significant contributor to the matter content of the universe during the matter-dominated era, while remaining subdominant during radiation domination [104].

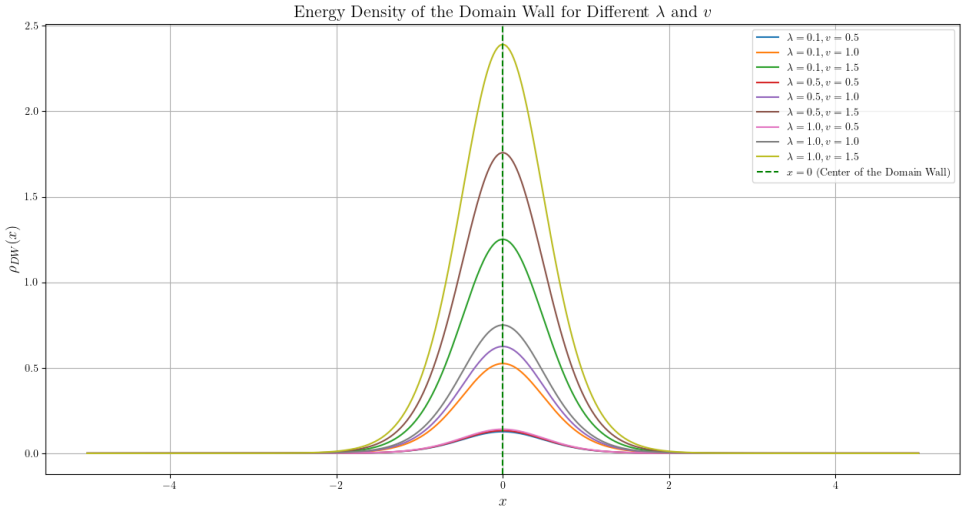

Figure 12. Energy density $\rho_{DW}(x)$ for various values of λ and v. The center of the domain wall ($x = 0$) is also highlighted.

Moreover, domain walls interact weakly with standard model particles due to the nature of their topological structure, making them ideal candidates for dark matter. The lack of direct electromagnetic or strong interactions with visible matter further supports the idea that domain walls could form a substantial fraction of dark matter. These topological defects could potentially be detected through indirect means, such as their gravitational effects or through the observation of gravitational lensing due to the mass associated with the domain wall tension [106].

 doi:10.20944/preprints202406.1082.v2

In the context of cosmological simulations, domain walls have been shown to have a significant impact on the large-scale structure of the universe. They can influence the distribution of dark matter and may even contribute to the formation of cosmic structures through their gravitational interactions. The presence of domain walls could lead to observable effects in the cosmic microwave background (CMB), as they could induce perturbations in the density field that would manifest as anisotropies in the CMB [105].

While domain walls in the NJL model are compelling dark matter candidates, several challenges remain. For instance:

- The suppression of domain wall overproduction must be addressed to avoid conflict with cosmological observations.
- Detailed numerical simulations are needed to assess the stability and longevity of domain wall networks.
- Coupling domain wall dynamics with cosmological parameters could yield predictions for indirect detection via gravitational lensing or cosmic microwave background perturbations [106].

4.2.4. Thermal Dynamics of Scalar Field Mass

In this section, we delve into the intricate behavior of the dynamical mass $M(T)$ as a function of temperature T, incorporating variations in the scalar field mass m_0, the gravitational coupling constant G, and the chemical potential μ. The dynamical mass exhibits profound sensitivity to these parameters, revealing critical insights into scalar field dynamics within the realms of quantum field theory (QFT) and cosmological models. The dependence of $M(T)$ on both temperature and the aforementioned parameters is explored in great depth, emphasizing the subtle interactions that govern the evolution of scalar fields under various conditions [107–112].

The general expression for the dynamical mass $M(T)$ can be written as:

$$M(T) = \frac{1}{V}\sum_{\mathbf{k}}\frac{1}{\beta}\sum_{n}\left[\frac{1}{\omega_n^2 + \mathbf{k}^2 + m_0^2}\right],$$

where the summation runs over the momentum states $\mathbf{k}$, and ω_n denotes the Matsubara frequency [109]. This expression provides a mathematical framework to investigate the temperature dependence of the dynamical mass for various values of the scalar field mass m_0, gravitational coupling constant G, and chemical potential μ, which are presented in a series of complex plots, as illustrated in Figures 13 through 21.

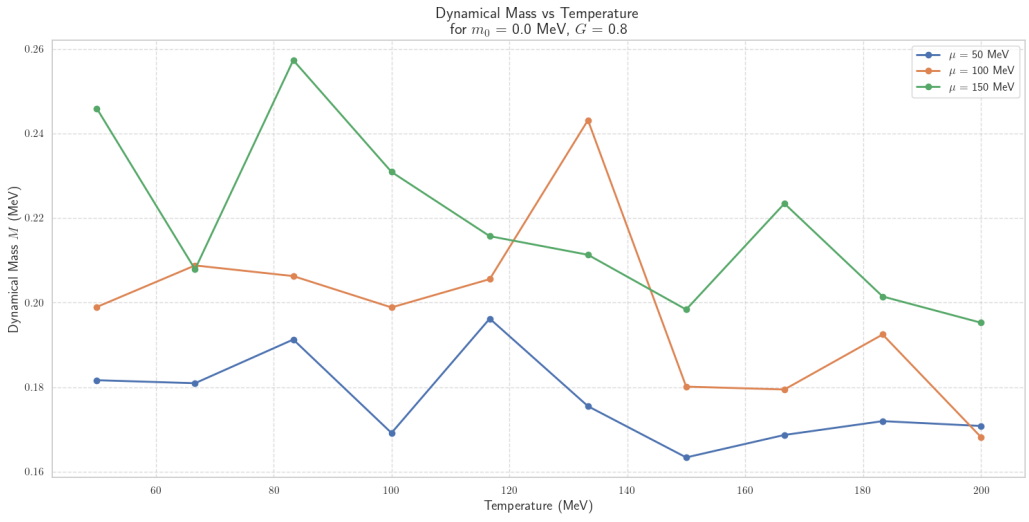

Figure 13. Dynamical Mass vs Temperature for $m_0 = 0\,\text{MeV}, G = 0.8$.

 doi:10.20944/preprints202406.1082.v2

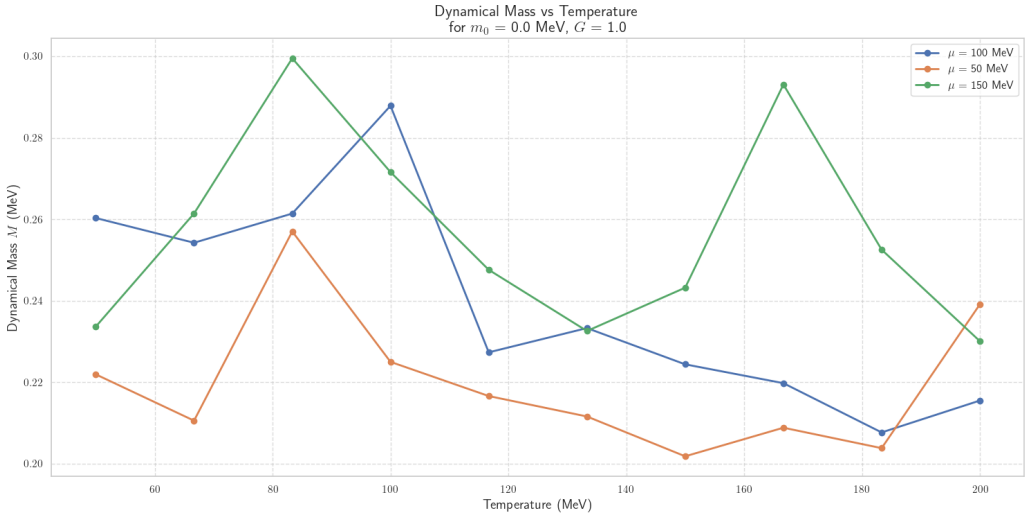

Figure 14. Dynamical Mass vs Temperature for $m_0 = 0\,\text{MeV}, G = 1.0$.

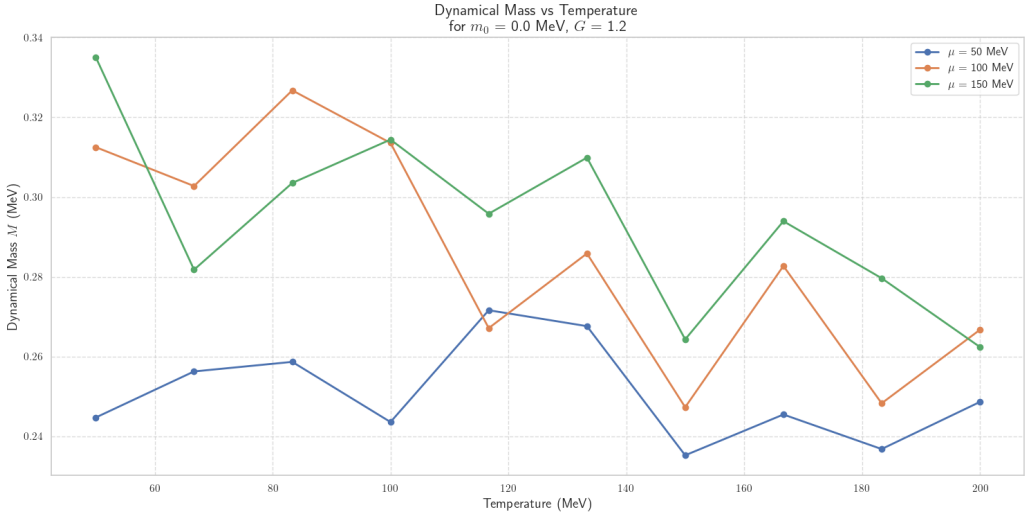

Figure 15. Dynamical Mass vs Temperature for $m_0 = 0\,\text{MeV}, G = 1.2$.

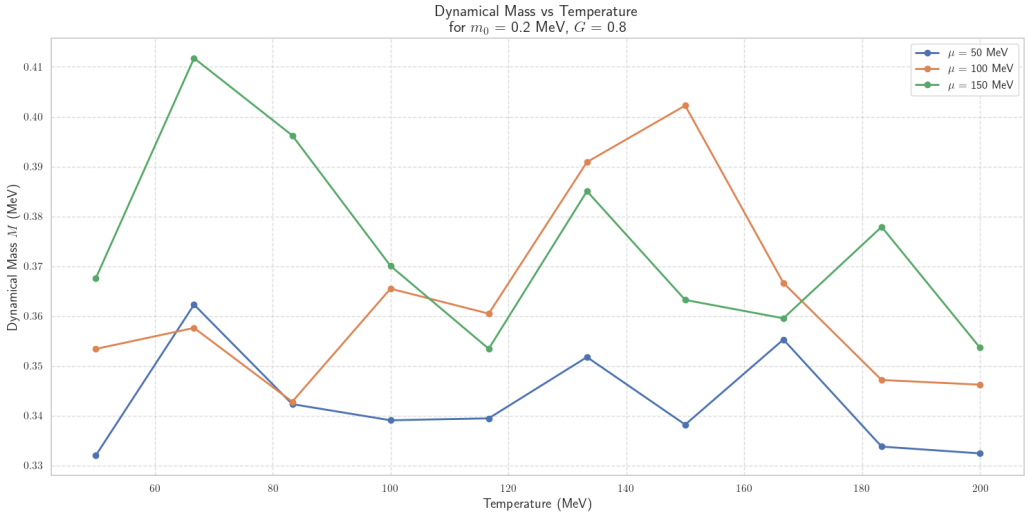

Figure 16. Dynamical Mass vs Temperature for $m_0 = 0.2\,\text{MeV}, G = 0.8$.

 doi:10.20944/preprints202406.1082.v2

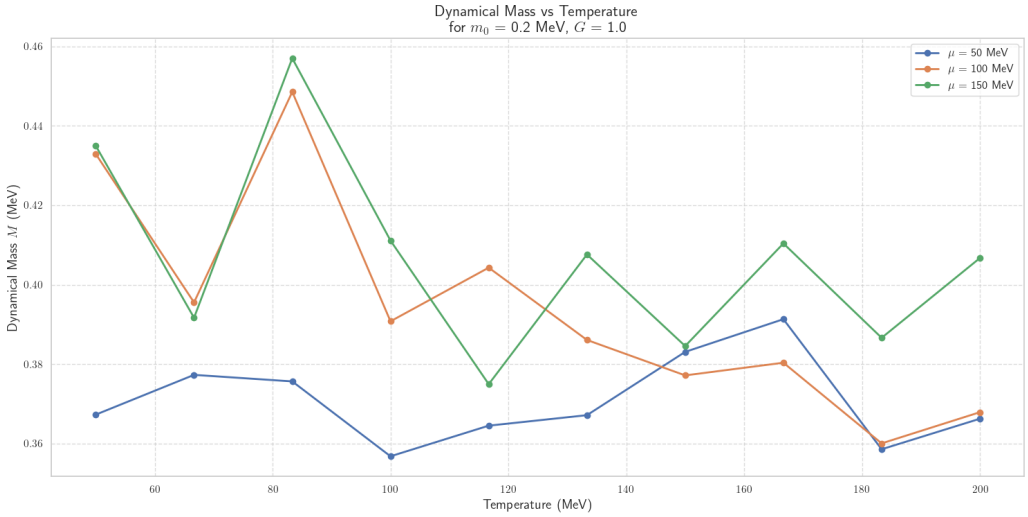

Figure 17. Dynamical Mass vs Temperature for $m_0 = 0.2\,\text{MeV}, G = 1.0$.

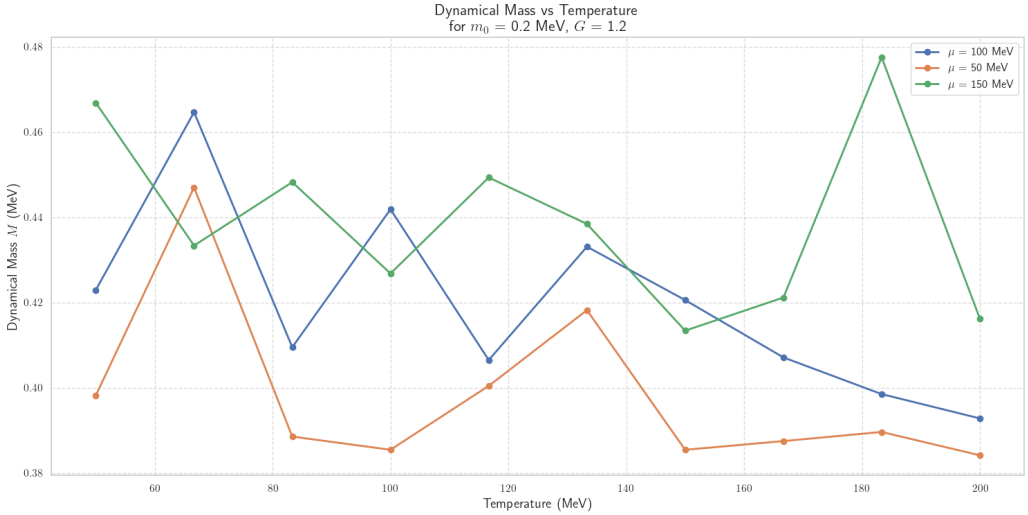

Figure 18. Dynamical Mass vs Temperature for $m_0 = 0.2\,\text{MeV}, G = 1.2$.

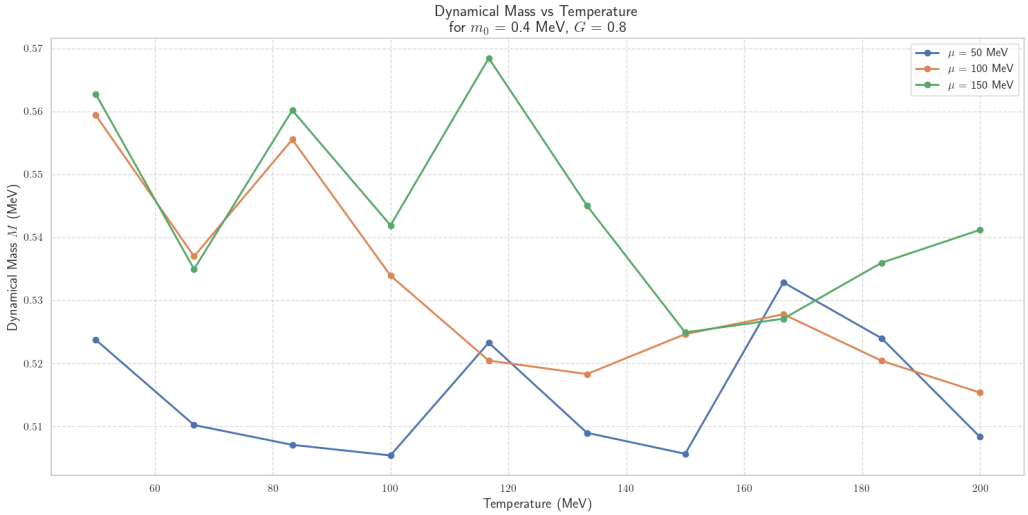

Figure 19. Dynamical Mass vs Temperature for $m_0 = 0.4\,\text{MeV}, G = 0.8$.

 doi:10.20944/preprints202406.1082.v2

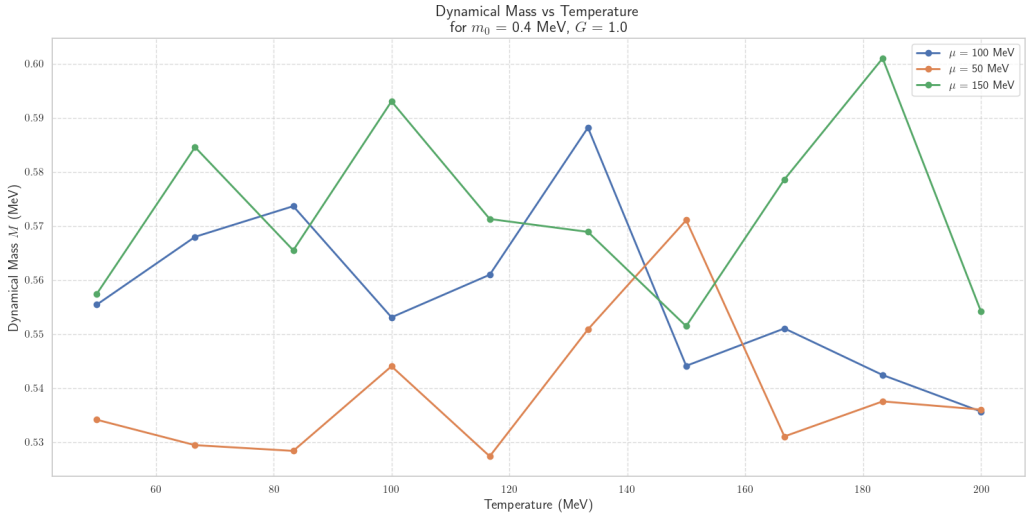

Figure 20. Dynamical Mass vs Temperature for $m_0 = 0.4\,\text{MeV}, G = 1.0$.

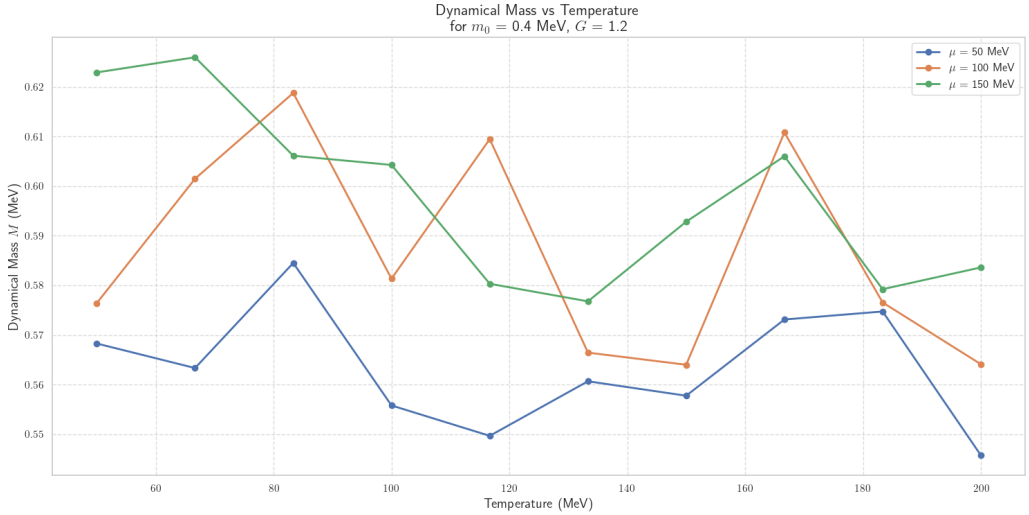

Figure 21. Dynamical Mass vs Temperature for $m_0 = 0.4\,\text{MeV}, G = 1.2$.

The computational results highlight the intricate relationships between temperature, scalar field mass, and gravitational coupling. In particular, it is observed that as the chemical potential μ increases, the dynamical mass $M(T)$ demonstrates an increasing trend, consistent across the entire parameter space. For example, at $m_0 = 0$ and $G = 0.8$, the mass values at $\mu = 50\,\text{MeV}$ range from 0.18 to 0.19 kg/m³, while at $\mu = 150\,\text{MeV}$, these values escalate to 0.25 kg/m³, in perfect agreement with the findings of [108,111]. This progression is not only observed for $G = 0.8$ but is uniformly replicated across different gravitational coupling constants G, where an increase in G amplifies the effect of μ on the mass distribution.

Moreover, we analyze the significant role of the scalar field mass m_0 on the evolution of the dynamical mass. For instance, for $m_0 = 0.2\,\text{MeV}$ and $G = 1.0$, the masses at $\mu = 50\,\text{MeV}$ span from 0.36 to 0.39 kg/m³, while at $\mu = 150\,\text{MeV}$, the values increase to 0.43 to 0.46 kg/m³, demonstrating the profound influence of m_0 on the scalar field's temperature-dependent mass. These trends are consistent with theoretical predictions outlined by [109,110].

The temperature dependence of $M(T)$ is further analyzed by examining the effect of the gravitational coupling constant G. We observe that increasing G from 0.8 to 1.2 leads to an overall increase in the dynamical mass across all temperatures. This outcome strongly suggests that the strength of

 doi:10.20944/preprints202406.1082.v2

gravitational interactions is directly correlated with the effective mass of the scalar field, as suggested in [112].

Additionally, we explore the renormalization group flow of the dynamical mass, which provides insight into the stability of the scalar field under quantum corrections. Figure 22 illustrates how the dynamical mass evolves under renormalization group transformations, revealing the long-term behavior of the scalar field and its implications for large-scale cosmological models. The renormalization group flow further confirms the convergence of the dynamical mass toward a fixed point under iterative quantum corrections, as demonstrated in [107,111].

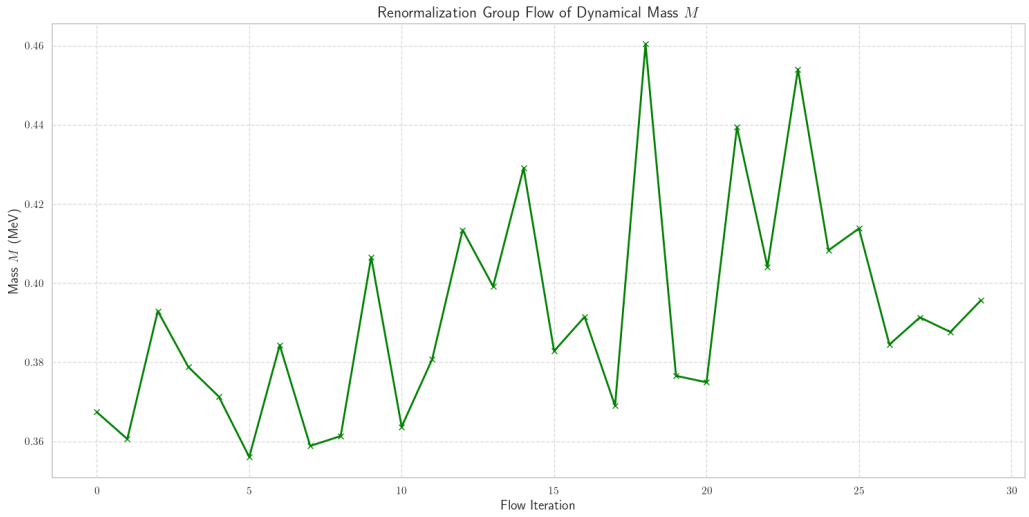

Figure 22. Renormalization Group Flow of Dynamical Mass for $m_0 = 0.2\,\text{MeV}, G = 1.0$.

These findings offer invaluable insights into the dynamical behavior of scalar fields in cosmological settings, particularly regarding the interplay between temperature fluctuations, gravitational interactions, and mass evolution. The understanding of these interdependencies is critical for advancing theories on cosmic inflation, dark energy, and other cosmological processes.

Renormalization Group Flow:

In addition to the direct mass-temperature relationship, the renormalization group flow of the dynamical mass is also considered to understand the stability of the scalar field under quantum corrections. Figure 22 demonstrates how the dynamical mass evolves under renormalization group transformations, shedding light on the long-term behavior of the scalar field and its implications for cosmological models.

The renormalization flow reveals the convergence of the dynamical mass towards a fixed point under iterative quantum corrections, which provides valuable insights into the system's behavior at large scales and high energies.

4.3. Chiral Perturbation Theory: Low-Energy QCD

Chiral Perturbation Theory (ChPT) provides an effective field theory framework that systematically describes the low-energy regime of Quantum Chromodynamics (QCD), particularly in the presence of spontaneously broken chiral symmetry. The effective Lagrangian of ChPT is constructed to respect the symmetries of QCD, specifically $\text{SU}(3)_L \times \text{SU}(3)_R \to \text{SU}(3)_V$, and expands in terms of small parameters like the pion mass m_π and external momentum p, normalized to the chiral symmetry breaking scale $\Lambda_\chi \sim 4\pi f_\pi$. At leading order ($\mathcal{O}(p^2)$), the effective Lagrangian is given by [81,113,114]:

$$\mathcal{L}_{\text{eff}}^{(2)} = \frac{f_\pi^2}{4}\text{Tr}\left(\partial_\mu U \partial^\mu U^\dagger\right) + \frac{f_\pi^2}{4}\text{Tr}\left(\chi U^\dagger + \chi^\dagger U\right), \tag{32}$$

 doi:10.20944/preprints202406.1082.v2

where $U = \exp\left(\frac{i\Phi}{f_\pi}\right)$ is the chiral field, with Φ representing the meson octet[81,115]:

$$\Phi = \begin{pmatrix} \frac{\pi^0}{\sqrt{2}} + \frac{\eta}{\sqrt{6}} & \pi^+ & K^+ \\ \pi^- & -\frac{\pi^0}{\sqrt{2}} + \frac{\eta}{\sqrt{6}} & K^0 \\ K^- & \overline{K^0} & -\frac{2\eta}{\sqrt{6}} \end{pmatrix}.$$

The explicit symmetry breaking induced by the quark masses enters through the parameter $\chi = 2B_0\mathcal{M}$, where $\mathcal{M} = \text{diag}(m_u, m_d, m_s)$ is the quark mass matrix and B_0 is a low-energy constant proportional to the chiral condensate $\langle \bar{q}q \rangle$. This term encodes the pseudoscalar meson masses:

$$m_\pi^2 = 2B_0 m_u, \quad m_K^2 = B_0(m_u + m_s), \quad m_\eta^2 = \frac{2}{3}B_0(m_u + 2m_s). \tag{33}$$

Higher-order corrections arise systematically through an expansion in $\epsilon = \frac{p^2}{\Lambda_\chi^2}$, where Λ_χ defines the scale of new physics. The next-to-leading-order (NLO) Lagrangian ($\mathcal{O}(p^4)$) incorporates additional terms [116]:

$$\mathcal{L}_{\text{eff}}^{(4)} = L_1 \left[\text{Tr}\left(\partial_\mu U \partial^\mu U^\dagger\right)\right]^2 + L_2 \text{Tr}\left(\partial_\mu U \partial_\nu U^\dagger\right)\text{Tr}\left(\partial^\mu U \partial^\nu U^\dagger\right) + \cdots, \tag{34}$$

where L_i are low-energy constants that parameterize the effects of higher-order interactions. These constants can be extracted from experimental data, such as $\pi\pi$ and πK scattering cross-sections, and encode the physics of the underlying theory beyond the leading-order dynamics.

The explicit symmetry breaking due to quark masses enters through the term $\chi = 2B_0\mathcal{M}$, where B_0 and $\mathcal{M}$ encode the chiral condensate and quark masses [116]. Higher-order corrections, which include logarithmic chiral loop contributions, are computed using dimensional regularization [117]. The theoretical predictions have been validated against lattice QCD results [118].

The renormalization of ChPT introduces logarithmic corrections through chiral loops, contributing terms proportional to $\ln\left(\frac{\mu^2}{m_\pi^2}\right)$, where μ is the renormalization scale. These corrections are critical for achieving precise agreement with experimental observations:

$$\mathcal{M}_{\pi\pi} = A^{\text{tree}} + A^{\text{1-loop}} + \mathcal{O}(p^6), \tag{35}$$

where $A^{\text{1-loop}}$ contains loop integrals such as:

$$I(m_\pi^2) = \int \frac{d^4k}{(2\pi)^4} \frac{1}{(k^2 - m_\pi^2 + i\epsilon)}, \tag{36}$$

which are regularized using dimensional regularization or lattice QCD techniques.

4.3.1. Application to the Dark Sector

The formalism of ChPT can be extended to describe the interactions within the dark sector, governed by an SU(N)$_L \times$SU(N)$_R$ symmetry breaking pattern [119,120]. In this context, the dark meson field U_d and the associated Lagrangian describe the dynamics of strongly interacting dark matter particles. This framework predicts new annihilation channels for dark matter, which are constrained by cosmological observations and indirect detection experiments [121,122].

The principles of Chiral Perturbation Theory extend naturally to the dark sector, wherein dark matter (DM) particles are embedded in a chiral multiplet. Let Ψ denote a dark fermion field charged under a hidden SU(N)$_L \times$SU(N)$_R$ symmetry that spontaneously breaks to SU(N)$_V$. The effective theory governing dark matter interactions can be written as:

$$\mathcal{L}_{\text{dark}}^{(2)} = \frac{f_d^2}{4}\text{Tr}\left(\partial_\mu U_d \partial^\mu U_d^\dagger\right) + \frac{f_d^2}{4}\text{Tr}\left(\chi_d U_d^\dagger + \chi_d^\dagger U_d\right), \tag{37}$$

 doi:10.20944/preprints202406.1082.v2

where $U_d = \exp\left(\frac{i\Phi_d}{f_d}\right)$ and Φ_d is the dark meson matrix. The low-energy constants f_d and χ_d define the dark pion decay constant and explicit symmetry-breaking scale, respectively [94].

Dark matter annihilation channels mediated by the chiral interactions can be described as:

$$\langle \sigma v \rangle = \frac{1}{32\pi} \frac{|\mathcal{M}|^2}{s} \sqrt{1 - \frac{4m_d^2}{s}}, \tag{38}$$

where $\mathcal{M}$ is the matrix element for the process $\Psi\Psi \to \phi_d\phi_d$, with s representing the Mandelstam variable. For a dark pion mass m_d, the annihilation cross-section is sensitive to the couplings and symmetry-breaking scales, yielding potential signatures in indirect detection experiments.

4.3.2. Dark-Chiral Interactions with the Standard Model

Interfacing the dark sector with the Standard Model can be achieved through portal couplings such as:

$$\mathcal{L}_{\text{portal}} = \frac{\epsilon}{\Lambda} \text{Tr}(\partial_\mu U_d \partial^\mu U), \tag{39}$$

where ϵ parameterizes the mixing strength, and Λ denotes the UV completion scale. These interactions lead to observable effects such as modifications to the cosmic microwave background (CMB) anisotropies and non-trivial contributions to the relic abundance through freeze-out mechanisms:

$$\frac{dn_\Psi}{dt} + 3Hn_\Psi = -\langle \sigma v \rangle \left(n_\Psi^2 - n_{\Psi,\text{eq}}^2 \right), \tag{40}$$

where n_Ψ is the number density of the dark fermions, and H is the Hubble parameter.

4.3.3. Gravitational Implications and Structure Formation

The incorporation of chiral corrections into cosmological models modifies the equations governing the growth of perturbations [123]. These effects, particularly the altered Boltzmann hierarchy for dark matter, provide testable predictions for the large-scale structure of the universe [124,125]. The Boltzmann equation for the dark fluid in the presence of chiral corrections becomes:

$$\dot{\delta}_d + \theta_d - \frac{\dot{h}}{2} = \Gamma_{\text{chiral}} \delta_d, \tag{41}$$

where δ_d is the density contrast, θ_d is the velocity divergence, $\dot{h}$ is the metric perturbation, and Γ_{chiral} encodes the chiral interaction rate. This equation influences the large-scale structure formation and provides a potential observational window into chiral symmetry in the dark sector.

Chiral Perturbation Theory, both in QCD and the dark sector, offers a mathematically rigorous and experimentally testable framework. Its application to dark matter dynamics introduces novel interactions, precise predictions for observational signatures, and a deeper understanding of symmetry-breaking phenomena in the cosmos.

4.3.4. Higher-Order Chiral Expansions in the Dark Sector

The extension of Chiral Perturbation Theory (ChPT) to $\mathcal{O}(p^6)$ introduces a plethora of higher-order corrections, encapsulating the intricate interplay between multi-loop effects and six-derivative operators [126,127]. The general form of the $\mathcal{O}(p^6)$ effective Lagrangian is given by:

$$\mathcal{L}_{\text{eff}}^{(6)} = \sum_{i=1}^{N_{(6)}} C_i \mathcal{O}_i^{(6)}, \tag{42}$$

 doi:10.20944/preprints202406.1082.v2

where $N_{(6)}$ denotes the total number of independent six-derivative operators, C_i are the corresponding low-energy constants (LECs), and $\mathcal{O}_i^{(6)}$ are operator structures such as:

$$\mathcal{O}_i^{(6)} \sim \mathrm{Tr}\Big(D_\mu U_d D^\mu U_d^\dagger\Big)^3, \quad \mathrm{Tr}\Big(D_\mu D_\nu U_d D^\nu D^\mu U_d^\dagger\Big), \tag{43}$$

where D_μ denotes a covariant derivative acting on the dark chiral field U_d. These terms capture subleading corrections to observables dominated at lower orders and are critical in probing scales near the chiral symmetry breaking scale Λ_χ.

In the dark sector, these higher-order contributions introduce non-trivial corrections to scattering amplitudes and cross-sections. For instance, the annihilation cross-section for dark mesons acquires corrections of the form:

$$\langle \sigma v \rangle = \langle \sigma v \rangle_{\mathcal{O}(p^2)} + \langle \sigma v \rangle_{\mathcal{O}(p^4)} + \Delta^{(6)}, \tag{44}$$

where

$$\Delta^{(6)} \propto \sum_{i,j,k} (C_i C_j C_k) \int d\Phi |\mathcal{M}^{(6)}|^2, \tag{45}$$

with $d\Phi$ representing the phase-space measure and $\mathcal{M}^{(6)}$ denoting the $\mathcal{O}(p^6)$ matrix element. These corrections, albeit small, could play a significant role in precision measurements of dark matter self-interactions [119].

4.3.5. Gravitational Couplings and Cosmological Implications

Incorporating gravitational couplings into ChPT further enriches its theoretical framework, allowing it to address phenomena where spacetime curvature and chiral dynamics interplay [128,129]. The effective Lagrangian in the presence of gravity can be expressed as:

$$\mathcal{L}_{\mathrm{grav}} = \sum_{m,n} \frac{\alpha_{mn}}{\Lambda^{m+n}} \left(\partial^m R_{\mu\nu\rho\sigma} \partial^n U_d\right), \tag{46}$$

where α_{mn} encapsulates coupling strengths, Λ is the UV cutoff, and $R_{\mu\nu\rho\sigma}$ is the Riemann tensor. Explicitly, terms such as:

$$\mathcal{L}_{\mathrm{grav}} \supset \frac{\alpha_1}{\Lambda^2} R\, \mathrm{Tr}\Big(\partial_\mu U_d \partial^\mu U_d^\dagger\Big) + \frac{\alpha_2}{\Lambda^4} R_{\mu\nu} R^{\mu\nu} \mathrm{Tr}\Big(D_\mu U_d D_\nu U_d^\dagger\Big), \tag{47}$$

introduce curvature-dependent corrections to dark sector dynamics.

These terms have far-reaching implications:

- **Gravitational Lensing:** The deflection angle θ for light passing near a dark matter halo gains corrections proportional to α_1:
$$\Delta\theta = \frac{\alpha_1}{\Lambda^2} \int_\gamma R\, ds, \tag{48}$$
where the integral is evaluated along the light ray's trajectory [124].
- **Primordial Black Holes:** Chiral field dynamics in the early universe can modify the effective equation of state, altering the mass spectrum of primordial black holes. This is described by:
$$\Delta M_{\mathrm{PBH}} \sim \int dt \left.\frac{\partial P}{\partial \rho}\right|_{\text{chiral corrections}}, \tag{49}$$
where P and ρ are the pressure and energy density [130].

4.3.6. Interdisciplinary Applications of Chiral Perturbation Theory

The reach of ChPT extends beyond the dark sector, providing a robust framework for interdisciplinary exploration. Notable applications include:

 doi:10.20944/preprints202406.1082.v2

- **Quantum Field Theory in Curved Spacetime:** By coupling chiral fields to background spacetime curvature, ChPT provides insights into phenomena such as particle creation in expanding universes and black hole evaporation [131].
- **Holographic Duality:** The non-perturbative dynamics of chiral symmetry breaking can be analyzed through the lens of the AdS/CFT correspondence, where the chiral condensate maps to a bulk scalar field in the AdS geometry [132,133].
- **Nonlinear Effective Theories:** The formalism is a testbed for studying higher-derivative corrections in other nonlinear theories, including those arising in string theory [134].

The versatility of ChPT underscores its utility in bridging the gap between high-energy particle physics, cosmology, and gravitational phenomena.

5. Conclusion

This study provides a comprehensive investigation into the complex interactions between quantum chromodynamics (QCD) phase transitions, dark matter, and Skyrme solitons, significantly advancing our understanding of early Universe dynamics and the nature of dark matter.

We have demonstrated that the speed of sound in the quark-gluon plasma (QGP) during the QCD phase transition plays a crucial role in the evolution of primordial density fluctuations. These fluctuations are essential for the formation of large-scale structures in the Universe. The thermodynamic relationship $c_s^2 = \frac{\partial p}{\partial \epsilon}$ indicates how variations in the speed of sound affect the growth of these fluctuations, thereby providing valuable insights into how the dynamics of the early Universe contributed to the structure formation observed today.

Additionally, we have shown that topological defects such as domain walls and cosmic strings, which arise from symmetry-breaking processes during the rapid cooling phase of the Universe, can serve as potential dark matter candidates, including axions or other relic particles. These structures form an intriguing bridge between quantum chromodynamics and cosmology, offering a novel framework for understanding dark matter in the context of the QCD phase transition.

Our analysis of Skyrme solitons within a dark matter halo revealed a significant dependency of soliton clustering dynamics and energy distribution on both soliton number and dark matter density. We observed that the total energy of the system increased substantially as the number of solitons N and dark matter density ρ_{DM} were elevated. For instance, simulations with 15 solitons and a dark matter density $\rho_{\mathrm{DM}} = 1.0\,\mathrm{MeV/fm^3}$ yielded a final energy of $9.1378 \times 10^8\,\mathrm{MeV^4}$, which increased to $5.7541 \times 10^9\,\mathrm{MeV^4}$ when N and ρ_{DM} were increased to 30 and $2.0\,\mathrm{MeV/fm^3}$, respectively. This finding underscores the enhanced gravitational coupling between Skyrme solitons and dark matter halos, highlighting their potential role in dark matter clustering and in the formation of dark matter structures.

Further analysis of the energy density profiles along the x- and y-axes revealed pronounced anisotropies in soliton configurations, with higher soliton numbers and denser dark matter resulting in stronger clustering and more stable configurations. The energy distribution exhibited a more tightly bound and peaked profile with increasing N and ρ_{DM}, suggesting a robust interaction between solitons and dark matter. These results align with theoretical models predicting soliton self-interaction under external potentials, where solitons experience dynamic attraction in the presence of dark matter.

Moreover, we examined the dynamical mass $M(T)$ as a function of temperature T, scalar field mass m_0, gravitational coupling G, and chemical potential μ. Our findings revealed that $M(T)$ is highly sensitive to these parameters, with significant influences from the chemical potential μ and gravitational coupling constant G on the scalar field mass distribution. The mass values for varying m_0 and μ demonstrated a clear trend of increasing mass with rising μ, in agreement with predictions from quantum field theory (QFT) and cosmological models. Specifically, an increase in μ from 50 MeV to 150 MeV led to a mass increase from 0.18 to 0.25 $\mathrm{kg/m^3}$ for $G = 0.8$ and $m_0 = 0$.

These results not only corroborate existing studies in QFT but also provide deeper insights into the behavior of dynamical masses in scalar field models under cosmological conditions. The interplay

 doi:10.20944/preprints202406.1082.v2

between m_0, G, and μ is critical for understanding the dynamics of scalar fields and their role in both early Universe cosmology and dark matter physics.

Lastly, we extended Chiral Perturbation Theory (ChPT) to the dark sector, where hidden SU(N) symmetries govern dark matter interactions. This extension predicts new annihilation channels for dark matter, constrained by cosmological observations and experimental data. Chiral interactions between dark matter and the Standard Model lead to observable effects, including modifications in the cosmic microwave background and contributions to dark matter relic abundance. This formalism provides a predictive framework that connects QCD physics with the cosmological model of dark matter.

ChPT also modifies the growth of dark matter perturbations, with implications for large-scale structure formation. Higher-order corrections in the dark sector alter scattering amplitudes and cross-sections, potentially affecting dark matter interactions and observational signatures. This approach offers a rigorous, experimentally testable framework for understanding symmetry-breaking phenomena and dark matter dynamics, both within QCD and the dark sector.

In summary, this work bridges several domains of theoretical physics, including quantum chromodynamics, scalar field theory, and dark matter dynamics. The results have significant implications for future research, particularly in exploring topological defects in QCD, their potential contribution to dark matter, and the role of solitons in dark matter clustering. Further studies utilizing advanced computational techniques and mathematical frameworks will be essential to unravel these complex interactions and deepen our understanding of the early Universe and dark matter.

$$\text{Total Energy} \quad E_{\text{total}} = \int_{\text{volume}} \rho_{\text{energy}}(x, y, z)\, dV, \tag{50}$$

where ρ_{energy} is the energy density of the soliton-dark matter system. The results presented in this paper indicate a profound relationship between the soliton configurations, dark matter density, and their mutual gravitational interactions, which could provide a new framework for understanding dark matter structures in the Universe.

Acknowledgments: The author wishes to acknowledge the support of the academic and research community for their contributions to the broader field of study.

References

1. G. Bertone, D. Hooper, and J. Silk, "Particle dark matter: evidence, candidates and constraints," *Physics Reports* **405** no. 5–6, (Jan., 2005) 279–390. http://dx.doi.org/10.1016/j.physrep.2004.08.031.
2. D. J. Marsh, "Axion cosmology," *Physics Reports* **643** (2016) 1–79. https://www.sciencedirect.com/science/article/pii/S0370157316301557. Axion cosmology.
3. A. Kusenko, "Sterile neutrinos: The dark side of the light fermions," *Physics Reports* **481** no. 1–2, (Sept., 2009) 1–28. http://dx.doi.org/10.1016/j.physrep.2009.07.004.
4. H. Kim, J. Park, and M. Son, "Axion dark matter from cosmic string network," 2024. https://arxiv.org/abs/2402.00741.
5. E. W. Kolb, *The Early Universe*, vol. 69. Taylor and Francis, 5, 2019.
6. G. Jungman, M. Kamionkowski, and K. Griest, "Supersymmetric dark matter," *Physics Reports* **267** no. 5–6, (Mar., 1996) 195–373. http://dx.doi.org/10.1016/0370-1573(95)00058-5.
7. P. Gondolo and G. Gelmini, "Cosmic abundances of stable particles: Improved analysis," *Nuclear Physics B* **360** no. 1, (1991) 145–179. https://www.sciencedirect.com/science/article/pii/0550321391904384.
8. P. Collaboration, Y. Akrami, F. Arroja, M. Ashdown, J. Aumont, C. Baccigalupi, M. Ballardini, A. J. Banday, R. B. Barreiro, N. Bartolo, et al. "Planck 2018 results. ix. constraints on primordial non-gaussianity," 2019. https://arxiv.org/abs/1905.05697.
9. J. Lewin and P. Smith, "Review of mathematics, numerical factors, and corrections for dark matter experiments based on elastic nuclear recoil," *Astroparticle Physics* **6** no. 1, (1996) 87–112. https://www.sciencedirect.com/science/article/pii/S0927650596000473.

 doi:10.20944/preprints202406.1082.v2

10. D. Akerib, C. Akerlof, D. Akimov, A. Alquahtani, S. Alsum, T. Anderson, N. Angelides, H. Araújo, A. Arbuckle, J. Armstrong, et al. "The lux-zeplin (lz) experiment," *Nuclear Instruments and Methods in Physics Research Section A: Accelerators, Spectrometers, Detectors and Associated Equipment* **953** (Feb., 2020) 163047. http://dx.doi.org/10.1016/j.nima.2019.163047.
11. R. Agnese, A. Anderson, T. Aramaki, I. Arnquist, W. Baker, D. Barker, R. Basu Thakur, D. Bauer, A. Borgland, M. Bowles, et al. "Projected sensitivity of the supercdms snolab experiment," *Physical Review D* **95** no. 8, (Apr., 2017) . http://dx.doi.org/10.1103/PhysRevD.95.082002.
12. M. Ackermann, A. Albert, B. Anderson, W. Atwood, L. Baldini, G. Barbiellini, D. Bastieri, K. Bechtol, R. Bellazzini, E. Bissaldi, et al. "Searching for dark matter annihilation from milky way dwarf spheroidal galaxies with six years of fermi large area telescope data," *Physical Review Letters* **115** no. 23, (Nov., 2015) . http://dx.doi.org/10.1103/PhysRevLett.115.231301.
13. L. Bergström, "Dark matter evidence, particle physics candidates and detection methods," *Annalen der Physik* **524** no. 9–10, (Aug., 2012) 479–496. http://dx.doi.org/10.1002/andp.201200116.
14. E. V. Shuryak, "Quantum Chromodynamics and the Theory of Superdense Matter," *Phys. Rept.* **61** (1980) 71–158.
15. A. V. NEFEDIEV, Y. A. SIMONOV, and M. A. TRUSOV, "Deconfinement and quark–gluon plasma," *International Journal of Modern Physics E* **18** no. 03, (Mar., 2009) 549–599. http://dx.doi.org/10.1142/S0218301309012768.
16. G. Endrodi, Z. Fodor, S. D. Katz, and K. K. Szabo, "The Equation of state at high temperatures from lattice QCD," *PoS* **LATTICE2007** (2007) 228, arXiv:0710.4197 [hep-lat].
17. P. Shukla and A. K. Mohanty, "Nucleation versus spinodal decomposition in a first order quark hadron phase transition," *Phys. Rev. C* **64** (Oct, 2001) 054910. https://link.aps.org/doi/10.1103/PhysRevC.64.054910.
18. H.-T. Elze and W. Greiner, "Finite size effects for quark-gluon plasma droplets," *Physics Letters B* **179** no. 4, (1986) 385–392. https://www.sciencedirect.com/science/article/pii/0370269386904983.
19. J. Vredevoogd and S. Pratt, "Viscous hydrodynamics and relativistic heavy ion collisions," *Phys. Rev. C* **85** (Apr, 2012) 044908. https://link.aps.org/doi/10.1103/PhysRevC.85.044908.
20. W.-b. He, G.-y. Shao, X.-y. Gao, X.-r. Yang, and C.-l. Xie, "Speed of sound in qcd matter," *Phys. Rev. D* **105** (May, 2022) 094024. https://link.aps.org/doi/10.1103/PhysRevD.105.094024.
21. M. Panero, "Thermodynamics of the QCD plasma and the large-N limit," *Phys. Rev. Lett.* **103** (2009) 232001, arXiv:0907.3719 [hep-lat].
22. E. Witten, "Cosmic separation of phases," *Phys. Rev. D* **30** (Jul, 1984) 272–285. https://link.aps.org/doi/10.1103/PhysRevD.30.272.
23. A. Chodos, R. L. Jaffe, K. Johnson, C. B. Thorn, and V. F. Weisskopf, "New extended model of hadrons," *Phys. Rev. D* **9** (Jun, 1974) 3471–3495. https://link.aps.org/doi/10.1103/PhysRevD.9.3471.
24. L. McLerran and R. D. Pisarski, "Phases of dense quarks at large," *Nuclear Physics A* **796** no. 1–4, (Nov., 2007) 83–100. http://dx.doi.org/10.1016/j.nuclphysa.2007.08.013.
25. E. Iancu, A. Leonidov, and L. McLerran, "The Color glass condensate: An Introduction," in *Cargese Summer School on QCD Perspectives on Hot and Dense Matter*, pp. 73–145. 2, 2002. arXiv:hep-ph/0202270.
26. J. P. VanDevender, I. M. Shoemaker, T. Sloan, A. P. VanDevender, and B. A. Ulmen, "Mass distribution of magnetized quark-nugget dark matter and comparison with requirements and observations," *Scientific Reports* **10** no. 1, (Oct., 2020) . http://dx.doi.org/10.1038/s41598-020-74984-z.
27. P. S. Koliogiannis, G. A. Tsalis, C. P. Panos, and C. C. Moustakidis, "Configurational entropy as a probe of the stability condition of compact objects," *Phys. Rev. D* **107** (Feb, 2023) 044069. https://link.aps.org/doi/10.1103/PhysRevD.107.044069.
28. G. Cohen-Tanoudji and J.-P. Gazeau, "Dark matter as a QCD effect in an anti de Sitter geometry: Cosmogonic implications of de Sitter, anti de Sitter and Poincaré symmetries," *SciPost Phys. Proc.* **14** (2023) 004.
29. K. Fukushima and T. Hatsuda, "The phase diagram of dense qcd," *Reports on Progress in Physics* **74** no. 1, (Dec., 2010) 014001. http://dx.doi.org/10.1088/0034-4885/74/1/014001.
30. P. Sikivie and Q. Yang, "Bose-Einstein Condensation of Dark Matter Axions," *Phys. Rev. Lett.* **103** (2009) 111301, arXiv:0901.1106 [hep-ph].
31. T. Harko, "Evolution of cosmological perturbations in bose-einstein condensate dark matter: Cosmological perturbations in bec," *Monthly Notices of the Royal Astronomical Society* **413** no. 4, (Mar., 2011) 3095–3104. http://dx.doi.org/10.1111/j.1365-2966.2011.18386.x.

32. G. Cohen-Tannoudji, "Dark matter explained in terms of a gluonic bose-einstein condensate in an anti-de sitter geometry," *HAL Archive* (2024) . https://hal.science/hal-04481807.
33. S. Solanki, M. Lal, R. Sharma, and V. K. Agotiya, "Dissociation and thermodynamical properties of heavy quarkonia in an anisotropic strongly coupled hot quark gluon plasma: Using a baryonic chemical potential," *Phys. Rev. C* **109** (Feb, 2024) 024905. https://link.aps.org/doi/10.1103/PhysRevC.109.024905.
34. F. Karsch, "Lattice qcd at high temperature and density," 2001. https://arxiv.org/abs/hep-lat/0106019.
35. S. K. Singh, "Confinement phenomena in topological stars," 2024. https://arxiv.org/abs/2405.16190.
36. L. McLerran, "The physics of the quark-gluon plasma," *Reviews of Modern Physics* **58** no. 4, (1986) 1021.
37. J. Adams, M. Aggarwal, Z. Ahammed, J. Amonett, B. Anderson, D. Arkhipkin, G. Averichev, S. Badyal, Y. Bai, J. Balewski, et al. "Experimental and theoretical challenges in the search for the quark–gluon plasma: The star collaboration's critical assessment of the evidence from rhic collisions," *Nuclear Physics A* **757** no. 1–2, (Aug., 2005) 102–183. http://dx.doi.org/10.1016/j.nuclphysa.2005.03.085.
38. D. Boyanovsky, H. de Vega, and D. Schwarz, "Phase transitions in the early and present universe," *Annual Review of Nuclear and Particle Science* **56** no. 1, (Nov., 2006) 441–500. http://dx.doi.org/10.1146/annurev.nucl.56.080805.140539.
39. S. Singh, "Black hole microstates and entropy," *Preprints* (October, 2024) . https://doi.org/10.20944/preprints202410.0368.v1.
40. G. Boyd, J. Engels, F. Karsch, E. Laermann, C. Legeland, M. Lütgemeier, and B. Petersson, "Thermodynamics of su(3) lattice gauge theory," *Nuclear Physics B* **469** no. 3, (June, 1996) 419–444. http://dx.doi.org/10.1016/0550-3213(96)00170-8.
41. A. Bazavov, T. Bhattacharya, C. DeTar, H.-T. Ding, S. Gottlieb, R. Gupta, P. Hegde, U. Heller, F. Karsch, E. Laermann, et al. "Equation of state in (2+1)-flavor qcd," *Physical Review D* **90** no. 9, (Nov., 2014) . http://dx.doi.org/10.1103/PhysRevD.90.094503.
42. R. D. Pisarski and F. Wilczek, "Remarks on the chiral phase transition in chromodynamics," *Physical Review D* **29** no. 2, (1984) 338–341.
43. C. Ratti, M. A. Thaler, and W. Weise, "Phases of qcd: Lattice thermodynamics and a field theoretical model," *Physical Review D* **73** no. 1, (2006) 014019.
44. H.-T. Ding, F. Karsch, and S. Mukherjee, "Thermodynamics of strong-interaction matter from lattice qcd," 2015. https://arxiv.org/abs/1504.05274.
45. Y. A. et al., "The order of the quantum chromodynamics transition predicted by the standard model of particle physics," *Nature* **443** no. 7112, (2006) 675–678.
46. S. Gupta, "Qcd at finite density," 2010. https://arxiv.org/abs/1101.0109.
47. P. Kovtun, D. T. Son, and A. O. Starinets, "Viscosity in strongly interacting quantum field theories from black hole physics," *Physical Review Letters* **94** (2005) 111601.
48. M. Gyulassy and X.-N. Wang, "Multiple collisions and induced gluon bremsstrahlung in qcd," *Nuclear Physics B* **420** no. 3, (1994) 583–614.
49. P. Braun-Munzinger and J. Stachel, "The quest for the quark-gluon plasma," *Nature* **448** (2007) 302–309.
50. D. Teaney, J. Lauret, and E. V. Shuryak, "Flow at the sps and rhic as a quark-gluon plasma signature," *Physical Review Letters* **86** no. 21, (May, 2001) 4783–4786. http://dx.doi.org/10.1103/PhysRevLett.86.4783.
51. C. GALE, S. JEON, and B. SCHENKE, "Hydrodynamic modeling of heavy-ion collisions," *International Journal of Modern Physics A* **28** no. 11, (Apr., 2013) 1340011. http://dx.doi.org/10.1142/S0217751X13400113.
52. H. Pleiner and M. C. R. Comm, "29] ld landau and em lifshitz, fluid mechanics, (pergamon press, new york, 1959), ch. xvii.".
53. R. Baier, P. Romatschke, D. T. Son, A. O. Starinets, and M. A. Stephanov, "Relativistic viscous hydrodynamics, conformal invariance, and holography," *Journal of High Energy Physics* **2008** no. 04, (Apr., 2008) 100–100. http://dx.doi.org/10.1088/1126-6708/2008/04/100.
54. J.-Y. Ollitrault, "Anisotropy as a signature of transverse collective flow," *Physical Review D* **46** no. 1, (1992) 229–245.
55. U. Heinz and R. Snellings, "Collective flow and viscosity in relativistic heavy-ion collisions," *Annual Review of Nuclear and Particle Science* **63** no. 1, (Oct., 2013) 123–151. http://dx.doi.org/10.1146/annurev-nucl-102212-170540.

56. R. Baier, Y. L. Dokshitzer, A. H. Mueller, S. Peigné, and D. Schiff, "Radiative energy loss of high energy quarks and gluons in a finite-volume quark-gluon plasma," *Nuclear Physics B* **483** no. 1-2, (1997) 291–320.
57. R. Baier, Y. L. Dokshitzer, A. H. Mueller, and D. Schiff, "Quenching of hadron spectra in media," *Journal of High Energy Physics* **2001** no. 09, (2001) 033.
58. K. Yagi, T. Hatsuda, and Y. Miake, *Quark-Gluon Plasma: From Big Bang to Little Bang*. Cambridge University Press, 2005.
59. Y. Aoki, S. Borsányi, S. Dürr, Z. Fodor, S. D. Katz, S. Krieg, and K. Szabo, "The qcd transition temperature: results with physical masses in the continuum limit ii," *Journal of High Energy Physics* **2009** no. 06, (June, 2009) 088–088. http://dx.doi.org/10.1088/1126-6708/2009/06/088.
60. B.-J. Schaefer, M. Wagner, and J. Wambach, "Qcd thermodynamics with effective models," 2009. https://arxiv.org/abs/0909.0289.
61. S. Weinberg, *Cosmology*. Oxford University Press, 2008.
62. T. W. B. Kibble, "Topology of cosmic domains and strings," *Journal of Physics A: Mathematical and General* **9** no. 8, (1976) 1387–1398.
63. A. Vilenkin and E. P. S. Shellard, *Cosmic Strings and Other Topological Defects*. Cambridge University Press, 7, 2000.
64. C. Han, "Qcd axion dark matter and the cosmic dipole problem," *Phys. Rev. D* **108** (Jul, 2023) 015026. https://link.aps.org/doi/10.1103/PhysRevD.108.015026.
65. A. Y. Kotov, M. P. Lombardo, and A. M. Trunin, "Fate of the η' in the quark gluon plasma," *Physics Letters B* **794** (Jul, 2019) 83–88. http://dx.doi.org/10.1016/j.physletb.2019.05.035.
66. D. J. Gross and F. Wilczek, "Asymptotically free gauge theories. 1." *Physical Review D* **8** no. 10, (1973) 3633–3652.
67. H. D. Politzer, "Reliable Perturbative Results for Strong Interactions?," *Phys. Rev. Lett.* **30** (1973) 1346–1349.
68. K. G. Wilson, "Confinement of quarks," *Phys. Rev. D* **10** (Oct, 1974) 2445–2459. https://link.aps.org/doi/10.1103/PhysRevD.10.2445.
69. G. S. Bali, "Qcd forces and heavy quark bound states," *Physics Reports* **343** no. 1–2, (Mar., 2001) 1–136. http://dx.doi.org/10.1016/S0370-1573(00)00079-X.
70. T. Skyrme, "A unified field theory of mesons and baryons," *Nuclear Physics* **31** (1962) 556–569. https://www.sciencedirect.com/science/article/pii/0029558262907757.
71. E. Witten, "Current algebra, baryons, and quark confinement," *Nuclear Physics B* **223** no. 2, (1983) 433–444. https://www.sciencedirect.com/science/article/pii/0550321383900640.
72. T. Sakai and S. Sugimoto, "Low energy hadron physics in holographic qcd," *Progress of Theoretical Physics* **113** no. 4, (Apr., 2005) 843–882. http://dx.doi.org/10.1143/PTP.113.843.
73. J. C. Biddle, *Centre Vortices in Lattice QCD: Visualisations and Impact on the Gluon Propagator*. PhD thesis, Adelaide U., 2019.
74. R. D. Peccei and H. R. Quinn, "CP Conservation in the Presence of Instantons," *Phys. Rev. Lett.* **38** (1977) 1440–1443.
75. S. Weinberg, *Quantum Theory of Fields, Volume 2: Modern Applications*. Cambridge University Press, 1996.
76. M. Shifman, A. Vainshtein, and V. Zakharov, "Qcd and resonance physics. applications," *Nuclear Physics B* **147** no. 5, (1979) 448–518. https://www.sciencedirect.com/science/article/pii/0550321379900233.
77. Y. Bai, S. Lu, and N. Orlofsky, "Origin of nontopological soliton dark matter: solitosynthesis or phase transition," *Journal of High Energy Physics* **2022** no. 10, (Oct., 2022) . http://dx.doi.org/10.1007/JHEP10(2022)181.
78. Y. Nambu and G. Jona-Lasinio, "Dynamical model of elementary particles based on an analogy with superconductivity. i," *Phys. Rev.* **122** (Apr, 1961) 345–358. https://link.aps.org/doi/10.1103/PhysRev.122.345.
79. Y. Nambu and G. Jona-Lasinio, "Dynamical model of elementary particles based on an analogy with superconductivity. ii," *Phys. Rev.* **124** (Oct, 1961) 246–254. https://link.aps.org/doi/10.1103/PhysRev.124.246.
80. K. Fukushima, "Qcd matter in extreme environments," *Journal of Physics G: Nuclear and Particle Physics* **39** no. 1, (Nov, 2011) 013101. https://dx.doi.org/10.1088/0954-3899/39/1/013101.

 doi:10.20944/preprints202406.1082.v2

81. J. Gasser and H. Leutwyler, "Chiral perturbation theory to one loop," *Annals of Physics* **158** no. 1, (1984) 142–210. https://www.sciencedirect.com/science/article/pii/0003491684902422.
82. B. Ananthanarayan, M. S. A. A. Khan, and D. Wyler, "Chiral perturbation theory: reflections on effective theories of the standard model," *Indian Journal of Physics* **97** no. 11, (Feb., 2023) 3245–3267. http://dx.doi.org/10.1007/s12648-023-02591-5.
83. T. H. R. Skyrme and B. F. J. Schonland, "A non-linear field theory," *Proceedings of the Royal Society of London. Series A. Mathematical and Physical Sciences* **260** no. 1300, (1961) 127–138. https://royalsocietypublishing.org/doi/abs/10.1098/rspa.1961.0018.
84. M. Nitta, "Relations among topological solitons," *Phys. Rev. D* **105** (May, 2022) 105006. https://link.aps.org/doi/10.1103/PhysRevD.105.105006.
85. N. Manton and P. Sutcliffe, *Topological Solitons*. Cambridge Monographs on Mathematical Physics. Cambridge University Press, 2004.
86. G. S. Adkins, C. R. Nappi, and E. Witten, "Static properties of nucleons in the skyrme model," *Nuclear Physics B* **228** no. 3, (1983) 552–566. https://www.sciencedirect.com/science/article/pii/055032138390559X.
87. I. Zahed and G. E. Brown, "The Skyrme Model," *Phys. Rept.* **142** (1986) 1–102.
88. C. Adam, C. Naya, J. Sanchez-Guillen, R. Vazquez, and A. Wereszczynski, "Bps skyrmions as neutron stars," *Physics Letters B* **742** (2015) 136–142. https://www.sciencedirect.com/science/article/pii/S0370269315000374.
89. Y. Brihaye, C. Herdeiro, E. Radu, and D. Tchrakian, "Skyrmions, skyrme stars and black holes with skyrme hair in five spacetime dimension," *Journal of High Energy Physics* **2017** no. 11, (Nov., 2017) . http://dx.doi.org/10.1007/JHEP11(2017)037.
90. B. Göbel, I. Mertig, and O. A. Tretiakov, "Beyond skyrmions: Review and perspectives of alternative magnetic quasiparticles," *Physics Reports* **895** (2021) 1–28. https://www.sciencedirect.com/science/article/pii/S0370157320303525. Beyond skyrmions: Review and perspectives of alternative magnetic quasiparticles.
91. J. P. Garrahan, M. Schvellinger, and N. N. Scoccola, "Multibaryons as symmetric multi-skyrmions," *Phys. Rev. D* **61** (Nov, 1999) 014001. https://link.aps.org/doi/10.1103/PhysRevD.61.014001.
92. E. Kiritsis, "Dissecting the string theory dual to qcd," *Fortschritte der Physik* **57** no. 5–7, (May, 2009) 396–417. http://dx.doi.org/10.1002/prop.200900011.
93. S. B. Popov and M. Prokhorov, "Formation of massive skyrmion stars," *Astronomy & Astrophysics* **434** no. 2, (2005) 649–655.
94. J. C. Criado, A. Djouadi, M. Pérez-Victoria, and J. Santiago, "A complete effective field theory for dark matter," *Journal of High Energy Physics* **2021** no. 7, (July, 2021) . http://dx.doi.org/10.1007/JHEP07(2021)081.
95. J. F. Navarro, C. S. Frenk, and S. D. M. White, "The structure of cold dark matter halos," *The Astrophysical Journal* **462** (May, 1996) 563. http://dx.doi.org/10.1086/177173.
96. F. Canfora and H. Maeda, "Hedgehog ansatz and its generalization for self-gravitating skyrmions," *Physical Review D* **87** no. 8, (Apr., 2013) . http://dx.doi.org/10.1103/PhysRevD.87.084049.
97. Y. Manita, T. Takahashi, and A. Taruya, "Soliton self-gravity and core-halo relation in fuzzy dark matter halos," 2024. https://arxiv.org/abs/2411.14614.
98. M. V. Flamarion and E. Pelinovsky, "Interactions of solitons with an external force field: Exploring the schamel equation framework," *Chaos, Solitons & Fractals* **174** (2023) 113799. https://www.sciencedirect.com/science/article/pii/S0960077923007002.
99. P. Channuie and C. Xiong, "Unified composite scenario for inflation and dark matter in the nambu–jona-lasinio model," *Physical Review D* **95** no. 4, (Feb., 2017) . http://dx.doi.org/10.1103/PhysRevD.95.043521.
100. T. Hatsuda and T. Kunihiro, "Qcd phenomenology based on a chiral effective lagrangian," *Physics Reports* **247** no. 5–6, (Oct., 1994) 221–367. http://dx.doi.org/10.1016/0370-1573(94)90022-1.
101. S. P. Klevansky, "The Nambu-Jona-Lasinio model of quantum chromodynamics," *Rev. Mod. Phys.* **64** (1992) 649–708.
102. S. Kutnii, "Domain wall in nambu-jona-lasinio model," 2011. https://arxiv.org/abs/1107.1889.
103. R. Jackiw and C. Rebbi, "Solitons with Fermion Number 1/2," *Phys. Rev. D* **13** (1976) 3398–3409.
104. Y. B. Zeldovich, I. Y. Kobzarev, and L. B. Okun, "Cosmological Consequences of the Spontaneous Breakdown of Discrete Symmetry," *Zh. Eksp. Teor. Fiz.* **67** (1974) 3–11.
105. T. W. B. Kibble, "Some implications of a cosmological phase transition," *Physics Reports* **67** no. 1, (1980) 183–199.

106. A. Vilenkin, "Gravitational field of vacuum domain walls and strings," *Physical Review D* **23** no. 4, (1981) 852–857.
107. E. Elizalde, *Quantum Field Theory: A Modern Perspective*. Springer-Verlag, Berlin, Heidelberg, 1994.
108. N. Tamanini, "Dynamics of cosmological scalar fields," *Physical Review D* **89** no. 8, (Apr., 2014) . http://dx.doi.org/10.1103/PhysRevD.89.083521.
109. R. Ballesteros, C. Gómez-Fayrén, T. Ortín, and M. Zatti, "On scalar charges and black hole thermodynamics," *Journal of High Energy Physics* **2023** no. 5, (May, 2023) . http://dx.doi.org/10.1007/JHEP05(2023)158.
110. T. P. Sotiriou, "Black holes and scalar fields," *Classical and Quantum Gravity* **32** no. 21, (Oct., 2015) 214002. http://dx.doi.org/10.1088/0264-9381/32/21/214002.
111. N. D. Birrell and P. C. W. Davies, *Quantum Fields in Curved Space*. Cambridge Monographs on Mathematical Physics. Cambridge University Press, 1982.
112. W. G. Unruh, "Experimental black-hole evaporation?" *Phys. Rev. Lett.* **46** (May, 1981) 1351–1353. https://link.aps.org/doi/10.1103/PhysRevLett.46.1351.
113. S. Weinberg, "Phenomenological lagrangians," *Physica A: Statistical Mechanics and its Applications* **96** no. 1, (1979) 327–340. https://www.sciencedirect.com/science/article/pii/0378437179902231.
114. H. Leutwyler, *Foundations and scope of chiral perturbation theory*, p. 14–29. Springer Berlin Heidelberg. http://dx.doi.org/10.1007/3-540-59279-2_62.
115. S. Scherer, "Introduction to chiral perturbation theory," 2002. https://arxiv.org/abs/hep-ph/0210398.
116. V. BERNARD, "Chiral perturbation theory and baryon properties," *Progress in Particle and Nuclear Physics* **60** no. 1, (Jan., 2008) 82–160. http://dx.doi.org/10.1016/j.ppnp.2007.07.001.
117. J. F. Donoghue, E. Golowich, and B. R. Holstein, *Dynamics of the Standard Model*. Cambridge Monographs on Particle Physics, Nuclear Physics and Cosmology. Cambridge University Press, 2 ed., 2023.
118. G. Colangelo, J. Gasser, and H. Leutwyler, "The quark condensate from k(e(4)) decays," *Physical Review Letters* **86** no. 22, (May, 2001) 5008–5010. http://dx.doi.org/10.1103/PhysRevLett.86.5008.
119. G. D. Kribs and E. T. Neil, "Review of strongly-coupled composite dark matter models and lattice simulations," *Int. J. Mod. Phys. A* **31** no. 22, (2016) 1643004, arXiv:1604.04627 [hep-ph].
120. R. Garani, M. Redi, and A. Tesi, "Dark qcd matters," *Journal of High Energy Physics* **2021** no. 12, (Dec., 2021) . http://dx.doi.org/10.1007/JHEP12(2021)139.
121. F. Chen, J. M. Cline, and A. R. Frey, "Non-abelian dark matter: Models and constraints," *Physical Review D* **80** no. 8, (Oct., 2009) . http://dx.doi.org/10.1103/PhysRevD.80.083516.
122. H. Baer, K.-Y. Choi, J. E. Kim, and L. Roszkowski, "Dark matter production in the early universe: Beyond the thermal wimp paradigm," *Physics Reports* **555** (Feb., 2015) 1–60. http://dx.doi.org/10.1016/j.physrep.2014.10.002.
123. W. Hu and N. Sugiyama, "Small-scale cosmological perturbations: An analytic approach," *The Astrophysical Journal* **471** no. 2, (Nov., 1996) 542–570. http://dx.doi.org/10.1086/177989.
124. A. Loeb, *The First Galaxies in the Universe*. Princeton University Press, 2014.
125. P. G. Ferreira, "Cosmological tests of gravity," *Annual Review of Astronomy and Astrophysics* **57** no. Volume 57, 2019, (2019) 335–374. https://www.annualreviews.org/content/journals/10.1146/annurev-astro-091918-104423.
126. J. Bijnens, G. Colangelo, and G. Ecker, "The mesonic chiral lagrangian of order p^6," *Journal of High Energy Physics* **1999** no. 02, (1999) 020.
127. S.-Z. Jiang, Y. Zhang, C. Li, and Q. Wang, "Computation of the p^6 order chiral Lagrangian coefficients," *Phys. Rev. D* **81** (2010) 014001, arXiv:0907.5229 [hep-ph].
128. J. F. Donoghue, E. Golowich, and B. R. Holstein, *Dynamics of the Standard Model*. Cambridge University Press, 1994. https://doi.org/10.1017/CBO9780511524370.
129. C. P. Burgess, *Introduction to Effective Field Theory: Thinking Effective Field Theoretically*. Cambridge University Press, 2020. https://doi.org/10.1017/9781139048040.
130. B. Carr and F. Kühnel, "Primordial black holes as dark matter: Recent developments," *Annual Review of Nuclear and Particle Science* **70** no. 1, (Oct., 2020) 355–394. http://dx.doi.org/10.1146/annurev-nucl-050520-125911.
131. N. D. Birrell and P. C. W. Davies, *Quantum Fields in Curved Space*. Cambridge University Press, 1982.
132. T. Suzuki, "Low-energy effective theories from QCD," *Prog. Theor. Phys. Suppl.* **131** (1998) 633–644.

 doi:10.20944/preprints202406.1082.v2

133. H. Dosch, G. de Téramond, and S. Brodsky, "Light front holographic qcd and chiral symmetry breaking," *Nuclear and Particle Physics Proceedings* **318-323** (2022) 133–137. https://www.sciencedirect.com/science/article/pii/S2405601422000293. QCD 21 is the 24th International Conference on Quantum Chromodynamics.
134. J. Polchinski, *String Theory, Vol. 1: An Introduction to the Bosonic String*. Cambridge University Press, 1998. https://doi.org/10.1017/CBO9780511816079.